AD-A073 871 ARNOLD ENGINEERING DEVELOPMENT CENTER ARNOLD AFS TN F/G 21/9.1
CONTAMINATION MEASUREMENTS FROM A 5 LB SUB F THRUST BIPROPELLAN--ETC(U)
JAN 79 R E ALT, H M POWELL, L L PRICE

UNCLASSIFIED AEDC-TSR-79-V4 NL

| OF |
AD
A073871

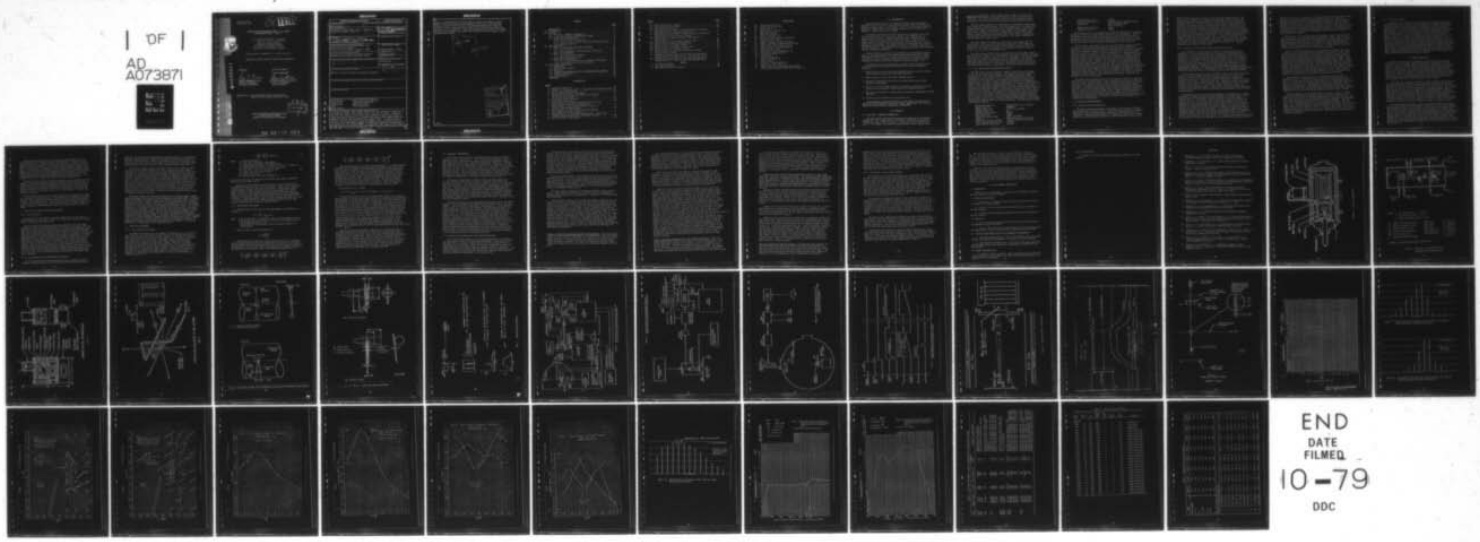

END
DATE FILMED
10-79
DDC

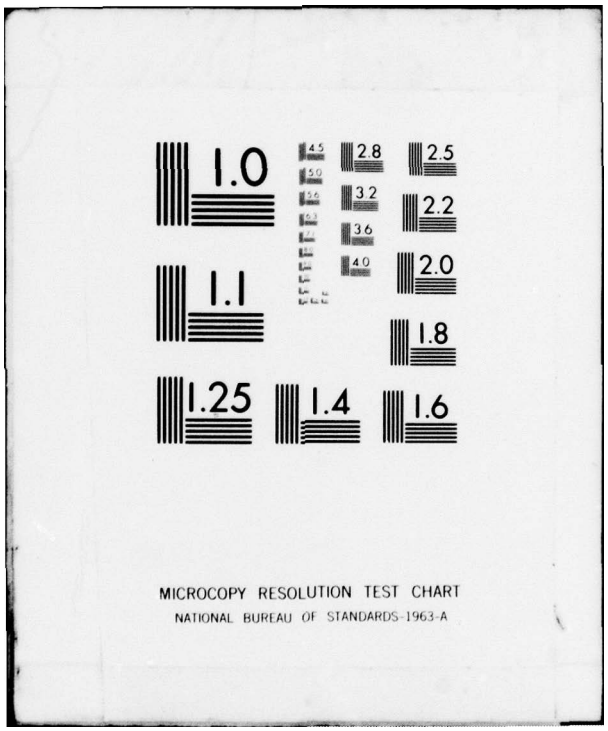
1.0
1.1
1.25
1.4
1.6
1.8
2.0
2.2
2.5
2.8
3.2
3.6
4.0
4.5
5.0
5.6
MICROCOPY RESOLUTION TEST CHART
NATIONAL BUREAU OF STANDARDS-1963-A

AEDC-TSR-79-V4
January 22, 1979

LEVEL II

CONTAMINATION MEASUREMENTS FROM A 5 lb_f THRUST BIPROPELLANT ENGINE - PHASE II

R. E. Alt, H. M. Powell, L. L. Price,
D. F. Frazine and W. B. Stephenson
ARO, Inc., AEDC Division
A Sverdrup Corporation Company
von Karman Gas Dynamics Facility
Arnold Air Force Station, Tennessee

Period Covered: September 25 - October 20, 1978

Approved for public release; distribution unlimited.

Reviewed By:

Larry F. Bowers

LARRY F. BOWERS, Capt, USAF
Test Director, VKF Division
Directorate of Test Operations

Approved for Publication:

FOR THE COMMANDER

James D. Sanders

JAMES D. SANDERS, Colonel, USAF
Director of Test Operations
Deputy for Operations

Prepared for: Air Force Rocket Propulsion Laboratory
Edwards Air Force Base, California 93523

ARNOLD ENGINEERING DEVELOPMENT CENTER
AIR FORCE SYSTEMS COMMAND
ARNOLD AIR FORCE STATION, TENNESSEE

REPORT DOCUMENTATION PAGE

READ INSTRUCTIONS BEFORE COMPLETING FORM

1. REPORT NUMBER: AEDC-TSR-79-V4	2. GOVT ACCESSION NO.
3. RECIPIENT'S CATALOG NUMBER	
4. TITLE (and Subtitle): Contamination Measurements from a 5 lb_f Thrust Bipropellant Engine - Phase II.	5. TYPE OF REPORT & PERIOD COVERED: Final Report, ~~September 25 - October 20, 1978~~
	6. PERFORMING ORG. REPORT NUMBER
7. AUTHOR(s): R. E. Alt, H. M. Powell, L. L. Price, D. F. Frazine, ~~and~~ W. B. Stephenson, ~~ARO, Inc., a Sverdrup Corporation Company~~	8. CONTRACT OR GRANT NUMBER(s)
9. PERFORMING ORGANIZATION NAME AND ADDRESS: Arnold Engineering Development Center (DO), Air Force Systems Command, Arnold Air Force Station, Tennessee 37389	10. PROGRAM ELEMENT, PROJECT, TASK AREA & WORK UNIT NUMBERS: Program Element 63411F
11. CONTROLLING OFFICE NAME AND ADDRESS: Air Force Rocket Propulsion Laboratory (PACP), Edwards Air Force Base, California 93523	12. REPORT DATE: January 22, 1979
	13. NUMBER OF PAGES: 49
14. MONITORING AGENCY NAME & ADDRESS (if different from Controlling Office): 11 22 Jan 79	15. SECURITY CLASS. (of this report): Unclassified
	15a. DECLASSIFICATION/DOWNGRADING SCHEDULE: N/A

16. DISTRIBUTION STATEMENT (of this Report)

Approved for public release; distribution unlimited. 12 52 p.

17. DISTRIBUTION STATEMENT (of the abstract entered in Block 20, if different from Report)

18. SUPPLEMENTARY NOTES

19. KEY WORDS (Continue on reverse side if necessary and identify by block number)

rocket engine	quartz crystal microbalance
electron beam	rotational temperature
contamination	laser scattering
plume	flow visualization
number density	

20. ABSTRACT (Continue on reverse side if necessary and identify by block number)

A Bipropellant Rocket Engine plume contamination test program was conducted in the Aerospace Chamber (10V) between Sept. 25 and Oct. 20, 1978. During the four week test period a 5-lb_f thrust rocket engine was fired over a range of engine operating parameters in a cryogenically pumped vacuum chamber where the background pressure was maintained below 1×10^{-5} torr. A vidicon image intensifier coupled spectrometer (VICS) system was used in conjunction with an electron beam to make number density and rotational temperature measurements of gas species (N_2, CO, CO_2 and H_2/H_2O) in the forward flow region of the rocket

DD FORM 1 JAN 73 1473 EDITION OF 1 NOV 65 IS OBSOLETE

• 000001 042 550

nozzle. A photomultiplier tube was used in place of the vidicon to make number density and temperature measurements of N_2 in the plume backflow region. Forward flow laser light scattering measurements were made with the VICS system to characterize the particle size and particle number distributions in the plume core. Mass flux measurements were made in the plume backflow region (60°-135° off axis) with cryogenically cooled quartz crystal microbalances (QCM's).

CONTENTS

ILLUSTRATIONS

NOMENCLATURE

A_e	nozzle exit area, in^2
A_T	nozzle throat area, in^2
B	bias limit, %
D	sonic orifice diameter, mm
f	QCM frequency, Hz
I	mass flux, gm/sec-sr
I_{sp}	specific impulse, sec
K	QCM calibration constant, gm/cm^2-Hz
$\dot{m}$	mass flow rate, gm/sec
N	number of pulses in firing sequence
P_c	engine combustion chamber pressure, psia
P_o	sonic nozzle total pressure, psia
R	radial distance, nozzle to QCM, cm
S	precision error index, %
T_o	sonic nozzle total temperature, ^oK
T_R	rotational temperature, ^oK
U	uncertainty, %
X	axial distance, mm
Y	vertical distance, mm
δ	duty cycle, %
τ_i	time of i^{th} data record, sec
τ_p	electrical pulse width, ms
ϕ	angle, plume axis to QCM aperture, degrees
Ω	solid angle subtended by QCM field-of-view, sr

1.0 INTRODUCTION

The work reported herein was conducted by the Arnold Engineering Development Center (AEDC) in the Aerospace Chamber (10V), von Karman Gas Dynamics Facility (VKF), at the request of the Air Force Rocket Propulsion Laboratory (AFRPL) under program element 62302F, Air Force Control No. 3058-00-8, and ARO Project No. V41Q-68.

The primary purpose of this test program was to provide a data base for the verification of an analytical computer code (CONTAM, Ref. 1) which attempts to model contaminant production and transport within a bipropellant rocket engine thrust chamber and plume. A 5 lb_f thrust rocket engine, developed by the Aerojet Corp. for the AFRPL (Ref. 2) was employed in the program. The engine analysis and design had been based on the CONTAM computer model which indicated that a low dribble volume multi-element injector was a prerequisite for attaining high pulse mode performance and low contaminant generation.

During the Phase I portion of the Bipropellant Contamination program (Ref. 3) the plume mass flux distribution was mapped with quartz crystal microbalances (QCM's) (Ref. 4) and a detailed study of the plume exhaust constituents in the solid phase ($26^{o}K$ and $77^{o}K$) was made with a Fourier transform spectrometer and laser diagnostic techniques (Refs. 5,6).

The objectives of this program were to obtain the following data for a specified engine configuration operating over a range of combustion parameters.

1. Number densities of N_2, CO, CO_2 and H_2/H_2O radially across the nozzle exit plane and axially along the plume centerline.

2. Number density of N_2 in the nozzle backflow region.

3. Rotational temperature of N_2 at all locations where the N_2 number density was determined.

4. Relative scattered light intensity from exhaust particulates near the plume axis as a function of time during the combustion profile.

5. Mass flux distribution of plume exhaust constituents condensible at $25^{o}K$ and $77^{o}K$.

6. Exhaust species identities near the plume axis.

A data package containing the Phase II test results was sent to the Air Force Rocket Propulsion Laboratory (PACP), Edwards Air Force Base, CA. Requests for data should be addressed to AFRPL/PACP.

2.0 APPARATUS

2.1 TEST UNIT - AEROSPACE CHAMBER 10V

The Bipropellant Contamination program was conducted in the Aerospace Chamber 10V. The chamber and its performance capability are described in general in Ref. 7 and in detail, as related to this test program, in Ref. 3. The chamber is designed for testing small rocket engines under

space vacuum conditions. The stainless steel chamber, located in the Engineering Laboratory Building of VKF, AEDC, is 10 ft in diameter and 20 ft long. The chamber is equipped with an internal cryogenic system designed for high efficiency vacuum pumping of rocket exhaust products.

The 10V chamber pumpdown is accomplished with mechanical vacuum pumps and a twenty-inch diffusion pump. The free expansion of the rocket plume is made possible by the high capture rate (pumping speed) of the exhaust gases on the chamber cryogenically cooled surfaces. The chamber cryogenic system consists of a liquid nitrogen (LN_2) cooled (77°K) chamber liner, a radial finned gaseous helium (GHe) cooled (20°K) cryopump and a liquid helium (LHe) cooled (4.2°K) cryopump. The chamber configuration for the program is shown in Fig. 1.

The rocket engine was located at the front of the chamber and was fired axially along the chamber horizontal centerline. The engine was installed in this position through an ante-chamber attached to the front of the 10V. The rocket engine nozzle was positioned nominally about 12 inches in front of the ante-chamber valve.

An electron beam (E-beam) source was installed on the chamber bottom, also 12 inches in front of the ante-chamber. The source directed the E-beam vertically into a Faraday cup at the top of the chamber. The vertical beam was aligned to bisect the exhaust plume just downstream of the nozzle. QCM's were attached to a GHe cooled line at locations in both the forward flow and backflow regions of the plume. One QCM was mounted directly on the chamber centerline in a region which also housed a mass spectrometer.

2.2 5 lb_f THRUST ENGINE AND PROPELLANT SYSTEM

The five-pound thrust bipropellant engine (AJ10-181) was developed by the Aerojet Liquid Rocket Company. The engine is designed to operate on nitrogen tetroxide (N_2O_4) oxidizer and monomethylhydrazine (MMH) ($CH_3N_2H_3$) fuel at a mixture ratio of 1.6 with propellant supply temperatures between 20°F and 120°F. The designated baseline (BL) engine configuration for the Phase II Biprop program was optimized for maximum performance with a pressure regulated propellant feed system and an uninsulated thrust chamber (combustion chamber-nozzle) (Ref. 8). This engine incorporates a 6-element splash plate injector (45 degree element orientation) and a 2-inch-long combustion chamber of cylindrical configuration with a 100:1 expansion ratio nozzle. This engine has no operating or duty cycle limitations at combustion chamber pressures to 110 psia (4 lb_f thrust) and will operate over a wide range of duty cycles at combustion chamber pressures up to 150 psia. During the engine development program (Ref. 2) the design goal specific impulse (I_{sp}) of 300 sec had been demonstrated for this engine configuration when operated in a steady state mode. The Bipropellant Engine Specifications follow.

Thrust (vacuum), lb_f	5 lb_f thrust at P_c = 140 psia
Propellants, O/F	N_2O_4/MMH
Mixture Ratio, O/F	1.4-1.8 (1.6 design)
Chamber Length, in.	2.0
Chamber pressure, psia	60-140
Area Throat, $in.^2$	0.0186
Nozzle Area Ratio, A_e/A_t	100:1, contoured
Injector	6-Element Splash Plate (45°)
Propellant Flow Rate, lb/sec	0.0167 lb/sec (P_c = 150 psia)
Inlet Pressure Oxidizer, psia	100-300
Inlet Pressure Fuel, psia	100-300

Dribble Volume, $in.^3$	0.0006
Nozzle/Chamber Material	Silicide-coated, Columbium Alloy
Application	Space Propulsion/RCS
	Free to Radiate
Minimum Pulse Duration	10 ms
Maximum Pulse Rate	25/sec

As previously noted, the bipropellant engine was mounted on a traversing mechanism located in an ante-chamber attached to the 10V chamber. The fuel and oxidizer run tanks, feedlines and pressure and flow rate measurement instrumentation were located along with the engine in the 10V ante-chamber. An isolation valve between the ante-chamber and 10V interior allowed access to the engine while the 10V chamber was maintained at test conditions.

Flexible tubing was provided for the fuel and oxidizer supply and drain lines and the GN_2 pressurization lines to the run tanks to allow the propellant feed system to move with the engine when the engine was traversed into firing position. Manual isolation valves were located in the supply and drain lines just exterior to the ante-chamber wall. The propellant run tanks were filled from 240 in^3 supply tanks located in propellant consoles near the chamber. Approximately 20 in^3 of propellant was transferred from the supply tanks to the run tanks initially and as the run tanks became depleted during testing. Figure 2 is a schematic of the propellant system. The propellant supply system from the run tanks to the engine conformed to the recommendations of Ref. 8 on feedline length and size and also pressure and flowrate measurement instrumentation. The engine operation was controlled by a millisecond (ms) sequencer which was programmed for bipropellant valve electrical pulse widths (EPW) and intervals between 1 and 9999 ms. Engine combustion chamber pressure (P_c), fuel and oxidizer flow rates, and feedline pressures were recorded on a CRT visicorder oscillograph, along with the bipropellant valve voltage pulse.

The engine was positioned axially in the chamber by means of a worm gear drive system in the ante-chamber. Axial position was indicated by means of an 18-in. scale, readable to ±0.10 inch, attached to the engine mount sting. The engine was primarily aligned to fire horizontally along the chamber centerline. All engine positioning was relative to the location determined for the electron beam nozzle profile number density measurements (approximately 12 inches from the ante-chamber door). Nozzle movement required from this location was retraction toward the ante-chamber up to 8 inches for electron beam axial profile number density measurements and extension of up to 4 inches and translation of 1.5 inches for electron beam backflow region number density measurements.

2.3 DIAGNOSTIC INSTRUMENTATION

2.3.1 Quartz Crystal Microbalances

The quartz crystal microbalance (QCM) (Refs. 9,10) used for the mass flux measurements is shown in Fig. 3. The electronics package is insulated from the mounting and independently temperature controlled at near room temperature. The crystal is mounted on a temperature controlled heat sink connected to the QCM mounting block by a thermal conductor sized to allow

$20^{o}K$ to $300^{o}K$ temperature cycling in one hour with a heater power of 10W. The QCM can be clamped to a constant low temperature $20^{o}K$ heat sink, the crystal temperature controlled anywhere between the heat sink temperature and $300^{o}K$, and the oscillator electronics maintained at room temperature. A field-of-view (FOV) limiting aperture, attached to the cover plate on the QCM, reduces the field-of-view to approximately $2\pi/12$ sr (48^{o} full angle), and thereby reduces the molecular flux reaching the crystal from directions other than the nozzle. The crystal temperature was taken to be that measured by a thermocouple imbedded in the heat sink to which the crystal was mounted. The temperature of the QCM surroundings was less than $80^{o}K$, excluding the thruster nozzle directly in the FOV, and as a result of radiation exchange between the QCM and its surroundings, the crystal temperature was calculated to be within $0.1^{o}K$ of the heat sink temperature. Typical QCM locations in the chamber are shown, relative to the plume axis, on Fig. 4. The QCM apertures were directed at the nozzle.

2.3.2 Electron Beam and Light Scattering Diagnostic System

The measurement technique and the composite instrument system were designed to fulfill the requirements for both gas and liquid drop phase diagnostics. A spatial map of gas species densities and N_2 temperatures in the forward flow , and N_2 densities and temperatures only in the backflow region, were to be measured and the presence of liquid drops in the forward flow was to be assessed. The low exit plane density values of the 100:1 area ratio nozzle dictated that the forward flowfield diagnostics, as well as the backflow region diagnostics, be performed using the electron beam fluorescence technique. The detection of liquid phase effluent required a high energy laser source to illuminate the flow. A spectrometer coupled light detection system was used for both liquid drop and gas phase measurements.

The integrated diagnostic system included a high energy (30 KV) electron beam source, synchronized electron beam sweep system, an electron beam collector assembly, pulse ruby laser (conventional mode) assembly and beam injection optics, laser beam receiver (energy dump), collection optics assembly, spectrometer, photomultiplier tube, intensifier-vidicon and readout-control devices, PDP-8 computer system, and an assortment of other control and data readout devices. In addition, a sonic orifice gas source was provided for calibration purposes. The subject devices were inter-connected to the thruster control system to synchronize the measurements with the engine firing sequence.

A description of the electron beam technique as a diagnostic for species densities and temperatures has been well documented elsewhere (Refs. 11-14). A description of the technique as used previously in the 10V chamber is noted in Ref. 11. The subject installation used a double spectrometer for spectral analysis of the fluorescence. Since both forward- and back-flow measurements were required and since these regimes were orders of magnitude different in density magnitude, two types of devices for the spectrometer detector were required. In the forward flow region the intensifier-vidicon system was used for density, temperature, and scattered light measurements. A photomultiplier tube (PMT) was used in the backflow region. The composite system including control and data acquisition devices was built around satisfying requirements of these devices. The volume of gas sample being viewed by the system is 3 mm wide, 6 mm high and 5 mm in depth and the output of the

photomultiplier tube is a measure of the integrated emission over that volume. The data were obtained using a photon counter, read by the computer to permanent storage along with other appropriate parameters. The intensifier-vidicon device was used as the forward flow detector system and was chosen because of its potential to obtain more data at a faster rate. With the appropriate optical collection system, the light could be collected according to a position in the flowfield corresponding discretely to a position on the vidicon detector. Thus spatial measurements could be made with individual data acquisition sequences.

Shown in Fig. 5 is the experimental arrangement. Both forward and back flow measurements were made with the installation as shown. Two electron beam collectors were required. The beam was directed vertically for forward flow measurements with the engine on centerline. Back flow measurements required pitching the electron beam to clear the nozzle and adjusting the engine elevation to provide for a radial scan. In each case the optics were focused at the centerline elevation of the electron beam.

Since the electron beam spread as it traversed the chamber from source to collector, it was determined that the electron beam must be swept across the slit image to ensure that the detectors see all of the beam current. This ensured that measurements in the rarefied portions of the plume (back flow) were in proper relation to the exit plane measurements, where potentially the beam spreading problems could give reduced signal levels. Figure 6 illustrates how the beam sweep was implemented with respect to the nozzle position and the spectrometer slit. The electron beam was swept across the image of the spectrometer slit which was located on the flow centerline and aligned perpendicular to the flow direction; i.e., the slit width was parallel to the plume axis and the slit height normal to the axis. Beam sweeping minimized the effects of electron beam spreading, due to both elastic and inelastic electron-molecule collisions, on the species densities.

The intensifier-vidicon output for a particular axial location is sketched in Fig. 7. To display the full nozzle exit diameter (1.47 in.) on the 0.5 in. diameter face of the intensifier a 0.3 optical magnification factor was used. The full diameter was imaged due to anticipated compression shocks in the flow field. The horizontal dimension or abscissa of the intensifier corresponds to wavelength; for a given radial position a horizontal intensifier read scan was performed to determine either the rotational temperature (T_R) of N_2 or the species densities of N_2, CO, CO_2, and H_2O.

A block diagram of the instrument system is shown in Fig. 8. Figures 9 and 10 are variations of the basic system required to accommodate the back flow and the light scattering measurements, respectively. Because each phase used common devices, the component units were assembled and programmed as a composite system, applicable to the desired measurement. Shown in Fig. 11 is a timing diagram of the data acquisition functions. The data delay, gate, and beam sweep function were obtained from a storage oscilloscope which was also used to monitor collector current or PMT output. The data gate was delayed following the start of the engine pulse to ensure data were acquired following the starting transient. The data gate was closed prior to pulse termination.

2.3.3 Mass Spectrometer

A quadrupole mass spectrometer was mounted on the chamber centerline behind the LN_2 baffle shielding the LHe cryopump. A skimmer was installed in the LN_2 baffle so that only a well defined beam of exhaust gas would pass through to the mass spectrometer. A sketch of this installation is shown in Fig. 12. The spectrometer assembly was attached directly to the LHe cryopump by means of an aluminum strut and was covered with a sheet metal housing bolted to the LHe cryopump. Also enclosed within this housing, and also attached to the LHe cryopump, was a quartz crystal microbalance which was so located to measure the centerline mass flux. An electrically operated shutter was installed to cover the skimmer apertures when it was desired to shield the instruments from the rocket exhaust. Due to problems encountered with chamber internal electronics wiring, the mass spectrometer could not be operated during the program. Pressure measurements made within the spectrometer housing indicated that the pressure at the sensing head was higher than the spectrometer operational limits and therefore a tighter enclosure would have been required for the mass spectrometer even had electronic problems not been encountered.

3.0 TEST DESCRIPTION

The Phase II portion of the Bipropellant Contamination program was conducted in the 10V chamber between September 18 and October 20, 1978. During the week of September 18-22 a 10V checkout pumpdown was conducted to verify the integrity of the chamber and pumping systems following modification and maintenance work on the chamber during the previous several months. No significant problems were encountered with chamber performance during this checkout; therefore a portion of the week was devoted to making preliminary signal level measurements with the intensified vidicon system, utilizing both the electron beam and pulsed laser interactions with the rocket plume to provide the optical signal to the vidicon.

A four-week test period was conducted between September 25 and October 20. The first week of this period was devoted to electron beam vidicon calibrations utilizing a sonic orifice with pure gases (N_2, CO, CO_2 and H_2) identical to the gas species to be mapped in the rocket plume. The following two weeks were devoted to the forward flow and backflow region species number density and rotational temperature (T_R) measurements. During the final week of testing the plume mass flux distribution was mapped utilizing the quartz crystal microbalances and the rocket plume scattered light intensity (from the pulsed laser source) was acquired on the vidicon system. A summary of the test matrix is contained in Table 1. Table 2 is an expansion of one portion of the matrix showing a single day's firing record.

The vidicon image intensifier coupled spectrometer (VICS) system was used for the forward flow measurements. Forward flow electron beam density and temperature profiles for N_2 across the exit plane at 13 radial positions and ten axial locations, respectively, were obtained out to greater than five nozzle diameters. Densities for CO, CO_2 and H_2/H_2O were obtained across the exit plane. The engine was also translated vertically up to one nozzle diameter and off-axis measurements were also made for N_2. Approximately 290 firings of one second duration were made to acquire this data. All firings were made with an engine combustion chamber pressure (P_c) of 100 psia. The O/F ratio was varied from the nominal 1.6 to high and low mixture ratios of 1.8 and 1.4.

Backflow region measurements of N_2 densities and temperatures in a region adjacent to the nozzle exit were also obtained. Because of sensitivity requirements, a photomultiplier tube was used as a detector for the backflow region measurements. All backflow region measurements were made with a 1.6 O/F ratio at a nominal 100 psia engine combustion chamber pressure. The relatively low densities in the backflow region required multiple engine pulses to acquire accurate signal levels for analysis. The majority of the data acquired with the photomultiplier tube detector in the exit plane/backflow region required 40 engine pulses of 250 ms duration. This pulsing was done at an engine duty cycle of 250 ms on, 9750 ms off.

Forward flow laser light scattering measurements were made with the VICS system. The measured scattered light intensities may be characteristic of liquid drop size and number distribution. Most of the data were obtained near the nozzle exit plane for 20 ms engine pulse widths. Data were also obtained throughout the combustion profile, including thrust buildup and tailoff, and at 5 ms intervals out to 50 ms after shutdown. Off-axis data were also acquired.

Mass flux measurements in the plume flow field were made with ten QCM's for a total of 39 pulse sequences. The majority of measurements were made with the QCM's operated at 25-26°K; several runs were made with the QCM's at 75°K. The measurements were very similar to those made during the Phase I portion of the test program. Data were acquired over a wider range of engine combustion chamber pressures and also for pulse widths as short as 10 ms.

3.1 TEST UNIT AND ENGINE OPERATING CONDITIONS

3.1.1 Test Conditions

The base pressure achieved in the 10V chamber prior to the start of engine firings was less than 1×10^{-6} torr. This base pressure was reached with or without the LHe pump filled.

The 10V chamber background pressure was monitored during all engine operations with a nude ionization gage located between the chamber wall and cryopanels. Other gages, located in the test volume just behind the engine, were only operated periodically since their operation added a singificant heat load to the small LHe cryopump in the front of the chamber. The pressure excursion experienced during pulse firing sequences ranged from the chamber base pressure to 1×10^{-5} torr, when the LHe pump was operating, for combinations of pulse widths of 200 ms or less, duty cycles of 10 percent or less, and all mixture ratio and P_c variations. The chamber background pressure rose to approximately 1×10^{-4} torr during the 1-second engine firings. Much of the data acquired at the exit plane and on axis in the forward flow region were acquired during engine firings made without the LHe pump operating. During these firings the chamber background pressure rose to near 1×10^{-3} torr. However, these measurements were made within the plume core where the plume expansion was not affected by the higher background pressure.

3.1.2 Data Acquisition and Measurement Uncertainty

The 5 lb_f bipropellant engine was operated at the feedline pressure settings contained in Ref. 8, which had been verified during the Phase I

program. The proper engine performance, P_c and O/F ratio, was reestablished with one-second engine performance firings made periodically as operating parameter changes dictated. Engine P_c transducer and fuel and oxidizer flow meter responses were recorded, along with the bipropellant valve operational voltage pulse, for every firing on a CRT visicorder oscillograph (Fig. 13).

The initial feedline pressure settings resulted in an engine P_c within 2 percent of the desired steady state level. Measured fuel and oxidizer flowrates were usually 5-10 percent below the steady-state levels calculated from Ref. 8. Minor adjustment to the feedline pressures were made based on the engine P_c and measured flowrates to obtain the desired P_c on subsequent firings. Reported P_c and O/F ratio are based on steady-state engine conditions. It must be recognized that for short pulse lengths neither P_c nor O/F were necessarily the levels reported, i.e., for a 10 ms pulse length with a desired P_c of 100 psia, the actual maximum P_c measured may be 65 psia, while the fuel and oxidizer flowrates could not be measured. The actual pressure response trace for the shortest pulses must be examined for the true pulse pressure history. The frequency response of the turbine flowmeter signal conditioners required that pulses of greater than one second be made in order to adequately measure flow rate.

During the longer pulse firing sequences made for backflow region number density measurement the engine injector temperature approached 300°F. An engine combustion chamber pressure decay was then noted as the pulse train continued. That is, from pulse to pulse a reduction in the maximum measured P_c of several psia would be noted. Normally for short pulse lengths there was no detectable difference in the peak pressure level measured from pulse to pulse. An adequate explanation of the cause of the decay was not made during testing. The decay could only be attributed to some heating effect that in turn created a decrease in one or both propellant flows. The P_c trace and flowmeter responses were normal during single pulse firings and on pulse sequences where the ignitor temperature did not approach 300°F. A posttest inspection of the engine revealed a leak at the engine combustion chamber pressure transducer boss on the injector. Since the leak was not evident pretest, the leak was probably created by the temperature cycling of the soldered connection on the injector. No data are presented for firings where the P_c decay was noted.

3.2 MASS FLUX MEASUREMENT

3.2.1 Data Acquisition Procedure

Ten QCM's were installed in the chamber by clamping them to a stainless steel cryogenic line at various locations (Fig. 4) to achieve angles (ϕ) of between 0 and 135 degrees from the plume centerline to the QCM's. The QCM's were always pointed at the nozzle. The cryogen line to which the QCM's were clamped was cooled with nominal 20°K GHe, allowing the QCM crystal temperature to be controlled from ~25°K to 300°K. When all of the QCM crystals had stabilized at the desired temperature, a set of QCM frequencies and temperatures was recorded; this was usually about ten minutes prior to the beginning of a sequence of engine firings. A second set was recorded just prior to the engine firing and a third set just after the firing sequence. If the data sets are designated 1, 2, and 3, respectively, the measured mass flux I is

$$I = \frac{d\dot{m}}{d\Omega} = \frac{KR^2 \Delta f}{N \tau_p}, \text{ gm/sec-sr} \quad (1)$$

where f = QCM beat frequency
$\dot{m}$ = mass rate collected by QCM, gm/sec
Ω = solid angle subtended by the QCM FOV, sr
K = QCM calibration constant = 1.77×10^{-8} gm/cm^2 - Hz (Ref. 9)
R = distance from nozzle exit to QCM crystal, cm
$\Delta f = (f_3 - f_2) - (f_2 - f_1)\, \tau_3 - \tau_2 / \tau_2 - \tau_1$, Hz (2)
N = number of engine firing pulses
τ_p = pulse length, sec
τ_i = time at which data were recorded, sec

The second term in Eq. (2) was used to eliminate the chamber background mass flux at each QCM location.

During the firing sequence, QCM frequencies were monitored with a frequency-to-voltage converter and a strip chart recorder. Data consisted of thermocouple voltages, QCM output frequencies, sample number, sample time, and engine firing particulars such as pulse length, duty cycle, number of pulses in the sequence, combustion chamber pressure, and O/F ratio. When one or more QCM's stopped oscillating due to mass saturation, normally at frequencies between 50 and 100 KHz, the crystals were heated to 300°K to remove the deposit. Mass flux measurements were made on a total of 39 firing sequences with the QCM's operating at either 25°K or 75°K. A typical mass flux data record is shown in Table 3.

3.2.2 Measurement Uncertainty

The uncertainty (U) of the mass flux measurement I (gm/cm^2-sr), is defined as

$$U = \pm (B + t_{0.95}\, S),$$

where B is the bias limit or systematic error in the measurement process
S is the precision error index, a function of the random error in the measurement process, and
t is the 95th percentile point of the two-tailed Students "t" distribution.

The mass flux, I, has been defined as

$$I = \frac{K\, R^2\, \Delta f}{N\, t_p}$$

The precision error and bias limits for the mass flux are calculated using the Taylor series expansion to approximate the effect of the errors in the measured values of the quantities in this equation on the parameter I. The precision error and bias limit of the mass flux I is given, in terms of the precision error and bias limits of the individual quantities, as:

$$\frac{S_I}{I} = \left(\left(\frac{S_K}{K}\right)^2 + \left(\frac{2S_R}{R}\right)^2 + \left(\frac{S_{\Delta f}}{\Delta f}\right)^2 + \left(\frac{S_N}{N}\right)^2 + \left(\frac{S_{\tau_p}}{\tau_p}\right)^2 \right)^{1/2}$$

$$\frac{B_I}{I} = \left(\left(\frac{B_K}{K}\right)^2 + \left(\frac{2B_R}{R}\right)^2 + \left(\frac{B_{\Delta f}}{\Delta f}\right)^2 + \left(\frac{B_N}{N}\right)^2 + \left(\frac{B_{\tau_P}}{\tau_P}\right)^2 \right)^{1/2}$$

The precision index of the mass flux measurement, I, is best estimated from the mass flux measurements made during the program rather than from precision error estimates of the individual quantities, even though there were insufficient data at identical test conditions to provide a strong statistical base. Several sets of data which include variations in test conditions that did not strongly affect the measured results were used to estimate the precision error. Five firing sequences were analyzed for six QCM angles with the QCM's operating at 25°K. The relative standard deviation at each angle ranged from 5.9 to 10.49%. Theprecision index of the QCM measurements was therefore estimated at ±10%. The degrees of freedom was taken as the number of firing sequences analyzed, five.

The uncertainty, U, is then:

$$U = \pm (B + t_{0.95}\, S) = \pm (B + 2.57\ (10)) = \pm (B + 25.7)\ \%$$

In analyzing the bias limit of the measurement process it is apparent that B_N, B_{T_p}, $B_{\Delta f}$ and B_R can be taken as zero. Certainly they are negligible when compared to the precision index, and probably also when compared to B_K, the bias limit of the QCM calibration constant (K). The value of K used in the present data reduction process is a theoretical value based entirely on the properties of the quartz crystal. A QCM calibration program conducted concurrently with the Phase II test program resulted in a calibration constant approximately 20 percent higher than the theoretical value. However, several effects have not been accounted for in the calibration which may, when evaluated, tend to provide closer agreement with the theoretical value. The effects that have not been accounted for are (1) the effect of the crystal temperature on the calibration constant; (2) the effect of the crystal temperature on the capture coefficient of the crystal for the gas species, mixtures, temperatures and densities encountered in the plume; and (3) the effect of the field-of-view limiting aperture on the measured flux. Using the bias of 20% the total uncertainty is then ±(20 + 25.7) or ±45.7 percent.

The QCM installed on the plume centerline did not function well in providing the desired centerline mass flux level. Except after long quiescent periods, with the LHe pump filled, the QCM temperature normally reached only the 25-26°K range. During the engine pulses the QCM recorded an instantaneous mass increase; however, there was a subsequent rapid reevaporization following the pulse and therefore only a small net gain in accumulated mass. It was obvious that the temperature of the crystal increased during the firing and that gases such as H_2O and CO_2 condensed, while N_2 and CO were only partially condensed. This resulted in an unknown measurement uncertainty with the centerline QCM.

3.3 DIAGNOSTIC MEASUREMENTS

The electron beam and laser scattering installation were available during the entire test sequence. The electron beam measurements were undertaken first, followed by the laser scattering measurements (Table 1). Upon completion of the laser scattering experiments, additional electron beam data were taken to supplement the original data. Generally all data were taken at 1.4, 1.6, and 1.8 O/F ratios at P_c = 100 psia. The additional case of a 1.4 O/F ratio at 75 psi was taken as an example of a "dirty" combustion process. For a given type of measurement, a prescribed pulse duration was used. Since the thruster pulse generally remained fixed, all intensity variations were handled by adjustment of the intensifier gain, the number of engine pulses, and with the use of optical filters.

The absolute measurements of number density and temperature made with the electron beam required the use of a heated sonic orifice for calibration purposes. The sonic orifice expansion is very well understood (Ref. 15) for given source conditions (pressure, temperature, and orifice diameter). Therefore density and temperature of the calibration gases were analytically determined. Appropriate calibration measurements were made intermittently during the course of the test. Only relative measurements were possible with the laser scattering system. However, a partial calibration was run in air at atmospheric conditions for an assessment of the Rayleigh component in the event particulate and droplet intensity levels were near background levels.

A detailed alignment of all components was performed before the chamber pumpdown. Finer adjustments were made after the chamber was at test conditions. The latter was accomplished by adjustment of the lens assemblies both internal and external to the chamber. Pre-pumpdown adjustments included alignment of the electron beam and laser axes along the vertical centerline of the thruster nozzle. The laser beam injection scheme is shown in Fig. 14. The collection optics alignment was made by focusing an illuminated point on a plumb bob at the thruster centerline reference position. Alignment for the backflow measurements was implemented in a similar fashion using instead a string between the "B" collector and the electron beam injection orifice (Fig. 5). Adjustments in the "B" collector were provided to assure that interception of the electron beam by the nozzle (including beam spreading effects) was eliminated. Included in pretest procedures was the alignment of the sonic orifice relative to the electron beam. The positioning mechanism included provision for making axial surveys of the orifice flow field, such that an accurate measurement of the position relative to the beam was possible.

3.3.1 Electron Beam Temperature and Density Measurement

The electron beam conditions were always established at 30 KV and 1 ma total current. After the beam system stabilized, a preferred focusing was obtained by selecting a balance between orifice current and beam spreading at the collector. After the beam was established in the appropriate collector (A or B depending upon whether forward- or backflow measurements were to be made), the sonic orifice flow was established. The optical alignment was then further refined; this generally involved only lateral and vertical adjustments in the external lens.

As noted earlier, beam sweeping was used so that the beam spreading effects could be minimized. To avoid unnecessary nozzle heating and to minimize the risk of nozzle damage, the sweep direction was in the direction of the nozzle. Sweep angle adjustments were thus required and selected to ensure that all the current swept across the slit image. At the same time the angle size was minimized to avoid unnecessary nozzle impingement and to maintain high signal levels. The beam sweeping technique and quenching effects limited how close to the nozzle the exit plane measurements could be made. The final adjustments in alignment were made by monitoring collector current and signal intensity simultaneously on the display oscilloscope while adjusting both to ensure coincidence of the respective peaks during beam sweeps.

All position measurements for both the thruster and sonic orifice were taken with respect to the line taken between the beam injection orifice and the collector cup. These measurements failed to hold after pumpdown, apparently because of the movement of the mounting hardware due to chamber wall cryogenic and vacuum loading. Sonic orifice calibrations provided the means of correcting position measurements for the movement encountered during the pumpdown/cooldown period.

The sonic orifice calibrations included measurements on N_2, CO_2, CO, and H_2. The intensity measurements, at known P_o and T_o, provided the means whereby the density of the respective components in the exhaust plume were determined.

The intensifier-vidicon sonic orifice measurements indicated that the sonic orifice had, upon chamber evacuation and cooling, shifted position relative to the electron beam in both the axial and transverse directions of the horizontal plane. In addition, the electron beam had shifted with respect to the optical line of sight. A good calibration was obtained, however, by performing an axial scan of the orifice and fitting the results to the known slope of the sonic orifice density expansion. That is, the experimental count rates were shifted in axial distance until the two slopes matched, thereby establishing the correct axial distances (Fig. 15). The typical departure from a good fit of experimental points to the calculated slope at low x/D is due to effects of quenching, alignment, and sharpness of radial peak profile. With the sonic orifice data and the calculated density expansion ratio at x/D = 18.70, a calibration factor was established. This number was assumed valid for all three days of the PMT back- and forward-flow measurements.

3.3.1.1 Forward Flow Intensifier--Vidicon Measurements. One- second sweep times were used for these measurements. The engine pulse time was slightly longer than one second to ensure that the beam sweep was completed before engine shut-down. Two engine pulses were required for each data point in a beam-on-beam-off sequence. The latter was subtracted from the former during data reduction in order to remove the background component from the data.

At a specific O/F ratio, all data required for determining the spatial variation of the densities and temperatures were taken. At fixed axial positions, all data for each specie were taken. This required specific wavelength selection for each specie of interest. For those species where potential spectral interference problems existed, several wavelength selections were used. In addition, multiple runs for N_2 were made using both resolved and unresolved spectra. This was done to verify the temperature measurements using the unresolved spectra. Data at axial locations out to 8 inches downstream from the nozzle were taken.

Sensitivity adjustments were made as required by intensifier gain selection. Usually a beam on-off sequence at test conditions would be taken for the purpose of establishing signal levels. A rapid recall capability was provided for data readout,on an oscilloscope display. In the event readjustments were required, a new intensifier voltage was selected. Multiple data input sequences were taken depending upon the signal levels relative to the noise component. The data reduction program had provision for co-adding spectra directly from the disk used for data storage.

Shown in Fig. 16 is a typical density profile for N_2 at 1.475 inch from the exit. These results are typical in that the peak value is near the centerline with the density falling off at the nozzle boundary layer region. When all centerline measurements were completed, off axis measurements were pursued. Shown in Fig. 17 are the off axis results for the same conditions noted previously. Noting that the data fall to zero at the edges, quite obviously some problem existed within the system. After analysis of the collection optics system it was determined that significant vignetting occurred, a case in which off axis radiation by-passed the focusing lens with increasing severity as the off axis distance increased. It was therefore necessary to post-calibrate with an optically flat field in order to correct the data. However, the entire radial profile could not be recovered since the signals at the extreme edges of the nozzle vanished. The flat field calibration for the original optical system configuration was made in order to provide corrections for the edge effect. A redesign of the optical system was then accomplished to provide the appropriate sensitivity at the nozzle edge positions. With this configuration, additional laser scattering and electron beam forward flow data were obtained. The electron beam data included the same measurements as noted earlier, except that only N_2 data were run because of limitations in test time. The optical system modification was essentially the removal of the internal chamber lens (Fig. 5), and the installation of a new lens external to the chamber (Fig. 8). The forward flow region density and temperature measurements made with the intensifier-vidicon (VICS) system are not included in this report. These data will be published later in an AEDC Technical Report.

3.3.1.2 Back Flow Photomultiplier Tube (PMT) Measurements. Back flow region measurements required replacing the intensifier system with a PMT and reducing the spectrometer slit height to 2 mm, corresponding to 6 mm in the flow field. The system configuration was also changed by using the "B" collector, raising, and moving the thruster forward. The spatial variations in the density and temperature measurements were accomplished with these two engine movements, corrected for the pitch in the electron beam.

The pulse time for PMT data acquisition was chosen as 0.25 sec. in order to keep the test chamber pressure as low as possible. Subsequently, for the very low density cases, multiple firings were used. Each pulse was separated by a 10-second interval. A delay to ensure engine stabilization was applied before initiating the 0.2-second sweep. The beam on-off sequence was also used for back flow PMT measurement. Again, engine pulse length was chosen slightly longer than 0.2 second to ensure that data gathering was completed before engine shutdown. Only nitrogen data were acquired in the back flow region. The ratio technique was used for the temperature measurement using a slit width consistent with unresolved spectra.

Scans were taken at fixed engine elevations a point at a time, with variations chosen in horizontal directions. The engine was moved forward at 0.25 inch intervals. Subsequent data were taken at intermediate points where large gradients existed. The extreme limits included those positions where there appeared to be a constant background density. The computer program was written such that pre-determined wavelengths were automatically selected and it was possible to obtain both temperature and density data at a given location.

Relatively intense and well-understood radiation from the interaction of beam electrons with nitrogen molecules was used for analysis of the nitrogen's number density and rotational temperature. Three wavenumbers in the N_2^+ First Negative System's (0,0) band and an adjacent background wavenumber were employed. Computer calculations with programs VIBTEMP and TROT were used to establish the correct band shapes as functions of vibrational and rotational temperatures, spectrometer dispersion, and slit widths.

Several scans of the (0,0) band were recorded during the sonic orifice measurements for a calibration of the spectrometer's wavenumber readout dial. Narrow slit widths produced the well-resolved rotational lines of accurately known wavenumbers. For the engine measurements, wide slit widths were used for sensitivity purposes.

Measured engine count rates were corrected for background and detector system dead time. Count rate ratios of the three wavenumbers were computed and compared with computer-calculated values to obtain rotational temperatures, and the resultant averaged values for the backflow region are shown in Fig. 18. To obtain number densities, the P branch wavenumber values were corrected by temperature-dependent bandshape factors and by collisional deactiviation, or quenching, factors. The results are shown in Fig. 19. The indicated engine axial coordinate has been shifted 0.35 inch over that measured when the chamber was warm and at atmospheric conditions. This amount of shift is subject to interpretation, and the justification for that used was the direction and position of the lines of constant number density. The radial coordinate is also subject to errors of the same cause but is shown unchanged.

3.3.1.3 Forward Flow PMT Measurements. Precisely the same procedure for data acquisition was followed in the forward flow PMT measurements as was used in the back flow, except that a fixed axial position was chosen, with variations in vertical direction (radial) in 0.125 inch steps. The near exit plane position was initially chosen with the same criterion as discussed in 3.3.1 pertaining to nozzle impingement and quenching.

Evaluation of the data near the exit plane indicated the existence of a shock. Since there were limitations in the time available to survey the flow field using the PMT technique, an axial centerline measurement was also made to help characterize the shock structure. The axial scan indicated a peak at 2 inches downstream. This position was in turn chosen for a radial survey. Off axis measurements were also pursued to complement tha back flow data around the nozzle and further downstream for rarefied boundaries of the plume. Axial and radial profiles of rotational temperature and number density are shown in Figs. 20, 21, 22 and 23. The axial coordinate has been shifted by the same 0.35 inch.

3.3.2 Laser Light Scattering Measurements

The system used for these measurements was essentailly that utilized for the electron beam forward flow measurements, except that the electron beam was replaced with a laser beam along the original beam axis. A laser energy "dump", which was positioned by means of a rotary feedthrough, was moved over the E-beam source. The beam collector assembly was similarly rotated out of position to allow injection of the laser beam into the nozzle test region. The laser injection optics were arranged such that the laser beam just filled the projected slit image (Fig. 14). External optics adjustments were required to optimize light collection. The spectrometer wavelength drive was set to 6943 Å. Signal sensitivity was selected by way of the intensifier gain.

The hardware arrangement provided for the capability of moving the data acquisition time anywhere within the thrust profile relative to the leading edge of the electrical pulse activating the thruster valve (Fig. 11). In addition, the data could be obtained after engine shut-down. The intensifier was turned on for 5 ms after the inserted delay and the laser triggered 2ms after the intensifier gate. The laser pulse was typically 800 μsec in length for the energy levels involved. The laser energy was chosen at a value large enough to ensure stability of energy and threshold delay.

An engine on-off sequence was followed for the data and background measurements, such that the difference would take into account any scattered laser light from system components. Measurements were also made with the engine on and laser off to ensure that background emission from the engine was inconsequential. Pretest and posttest data included measurements in air to take into account molecular scattering effects.

The relative measurements of scattered light intensity made during the combustion profile required a reference level. This reference measurement was chosen as the data point immediately before shut-down for a 100 ms pulse at 1.6 O/F ratio and 100 psia chamber pressure. The assumption was that with an extended pulse length, engine stabilization was established and this would represent a minimum contamination condition.

The reference data were for field 5, runs 354-358, as shown in Fig. 24. The peak occurring at field 5 instead of field 7 could be due to (1) a real effect, (2) positioning error, and (3) lack of application of channel sensitivity, or (4) combination of any of the above. Concerning item (3), application of the calibration rather than assuming all channels are of identical sensitivity tends to move the peak toward the center of the radial profile.

Shown in Fig. 25 is the composite data for fields 5 and 7 of runs 354-372. The time noted on the radial plot, such as Fig. 24 data, for the reference run is the delay before initiation of the data acquisition cycle which starts with turning on the intensifier. The actual time of data acquisition occurred 2.5 ms after the cycle was started. The composite plots for the respective data points of Fig. 25 has this time included. Figure 25a and b together represent the complete profile for a 100 ms engine pulse.

4.0 DATA PACKAGE PRESENTATION

4.1 PHOTOGRAPHS

Twenty-two still photographs of the Phase II test hardware installation are included in the data package.

4.2 ENGINE FIRING RECORDS

a. A record of all engine firings made during the Phase II program is included in the data package.

b. A copy of the test program Daily Operations Log is included in the data package.

c. A copy of engine firing oscillograph traces has been included in the data package.

4.3 MASS FLUX

a. The mass flux data records for the 39 data acquisition sequences are included in the data package.

b. Plots of mass flux as a function of direction from the plume axis for appropriately grouped parameters are included in the data package.

4.4 ELECTRON BEAM NUMBER DENSITY AND TEMPERATURE MEASUREMENTS

a. PMT Backflow Region Data. A log of all backflow region N_2 number density and temperature measurements is included in the data package.

b. PMT Forward Flow Region Data. A log of all exit plane and plume axis N_2 number density and temperature measurements is included in the data package.

4.5 LASER SCATTERING DATA

a. Composite relative scattered light intensity data plots for operating conditions listed in Table 1 for laser scattering measurements are included in the data package.

4.6 QCM CALIBRATION

A summary of the QCM calibration program is included in the data package.

REFERENCES

1. Hoffman, R. J., et al, "Plume Contamination Effects Prediction - the CONTAM Computer Program, Version II," AFRPL-TR-73-46 (1973).

2. Schoenman, L. and Schindler, R. C., "Five-Pound Bipropellant Engine," AFRPL-TR-74-51 (1974).

3. Alt, R. E., et al., "5 lb_f Thrust Bipropellant Engine Contamination Program - Phase I," AEDC-TR-79-28.

4. Scott, H. E., et al., "Bipropellant Engine Plume Contamination Study," USAF/NASA International Spacecraft Contamination Conference, March 7-9, 1978, U. S. Air Force Academy, Colorado.

5. Roux, J. A., et al., "IR Optical Properties of Bipropellant Contaminants," presented at USAF/NASA International Spacecraft Contamination Conference, March 7-9, 1978, U. S. Air Force Academy, Colorado.

6. Roux, J. A., et al., "Optical Properties of Bipropellant Exhaust Constituents Cryopumped at 77°K," presented at the AIAA 17th Aerospace Sciences Meeting, New Orleans, La., Jan. 15-17, 1979.

7. AEDC Facilities Handbook (Tenth Edition), Arnold Engineering Development Center, 1974.

8. Schoenman, L. and Lundgreen, R. B., "AJ10-181 5 lb_f Bipropellant Engine, Users Manual," Aerojet Liquid Rocket Company, Dec. 1976.

9. Baerwald, R. K. and Passamamech, R. W., "Monopropellant Exhaust Plume Contamination Measurements," AFRPL-TR-77-44 (1977).

10. Chirivella, J. E., "Hydrazine Engine Plume Contamination Mapping," AFRPL-TR-75-16 (1975).

11. Price, L. L., Powell, H. M. and Moskalik, R. S., "Species Number Density Measurements in Plume Interactions with Free Stream Using an Electron Beam Technique," AEDC-TR-71-226, November 1971.

12. Lewis, J. W. L. and Williams, W. D., "Electron Beam Fluorescence Diagnostics of a Ternary Gas Mixture," AEDC-TR-73-96, July 1973.

13. Limbaugh, C. C., Lewis, J. W. L., Kinslow, M., Powell, H. M., Price, L. L. and Williams, W. D., "Condensation of Nitrogen in a Hypersonic Nozzle Flow Field," AEDC-TR-74-31, May 1974.

14. Lewis, J. W. L., Williams, W. D., Price, L. L. and Powell, H. M., "Nitrogen Condensation in a Sonic Orifice Expansion Flow," AEDC-TR-74-36 (AD783254), July 1974.

15. Ashkenas, H. and Sherman, F. S. Rarefied Gas Dynamics, Fourth Symposium, Vol. II. Edited by J. H. deLeeuw. Academic Press, New York, 1966, pp. 84-105.

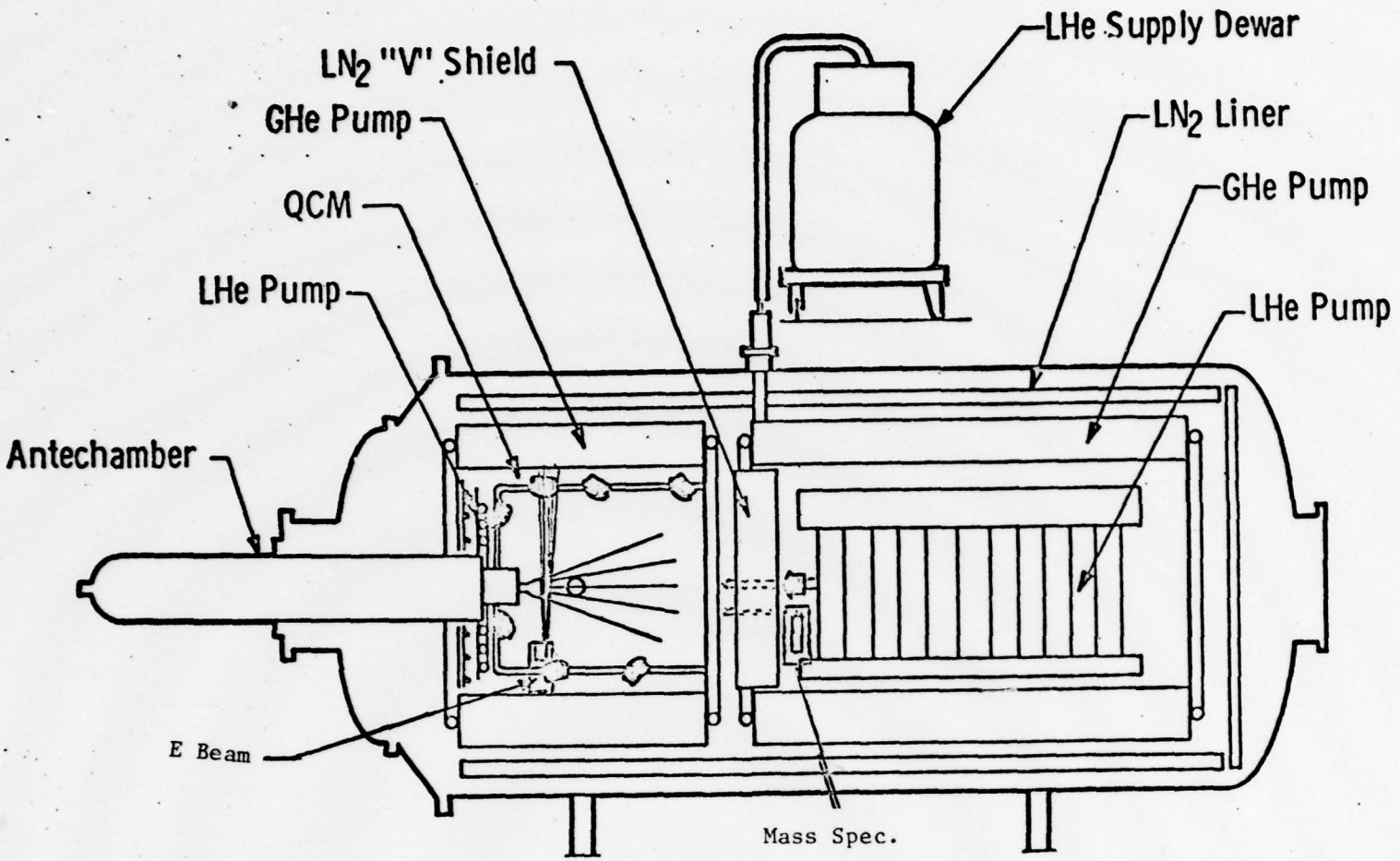

Figure 1 Aerospace Chamber 10V

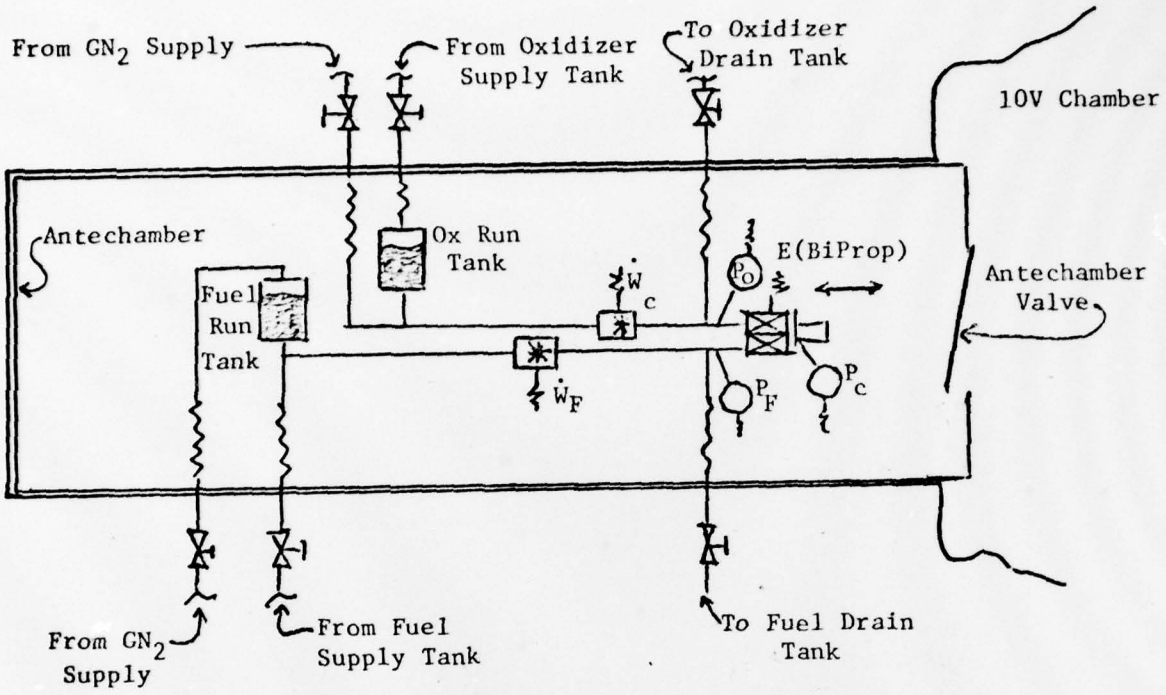

NOTES: 1. Run Tank Capacity 40 in^3.

2. Fuel Feedline Length 60 in.

3. Oxidizer Feedline Length 33 in.

P_c	Combustion Chamber Pressure	Taber 2210	0 - 200 psia
P_o	Oxidizer Feedline Pressure	Taber 2210	0 - 1000 psia
P_F	Fuel Feedline Pressure	Taber 2210	0 - 500 psia
$\dot{W}_o$	Oxidizer Flow Rate, gpm	Flow Technology	0 - 0.05 gpm
$\dot{W}_F$	Fuel Flow Rate, gpm	Flow Technology	0 - 0.05 gpm
E	Bipropellant Valve Voltage		0 - 28 VDC

Recorder: Honeywell Model 1858 CRT Visicorder

Figure 2 Schematic - Propellant System -- Bipropellant Contamination Test

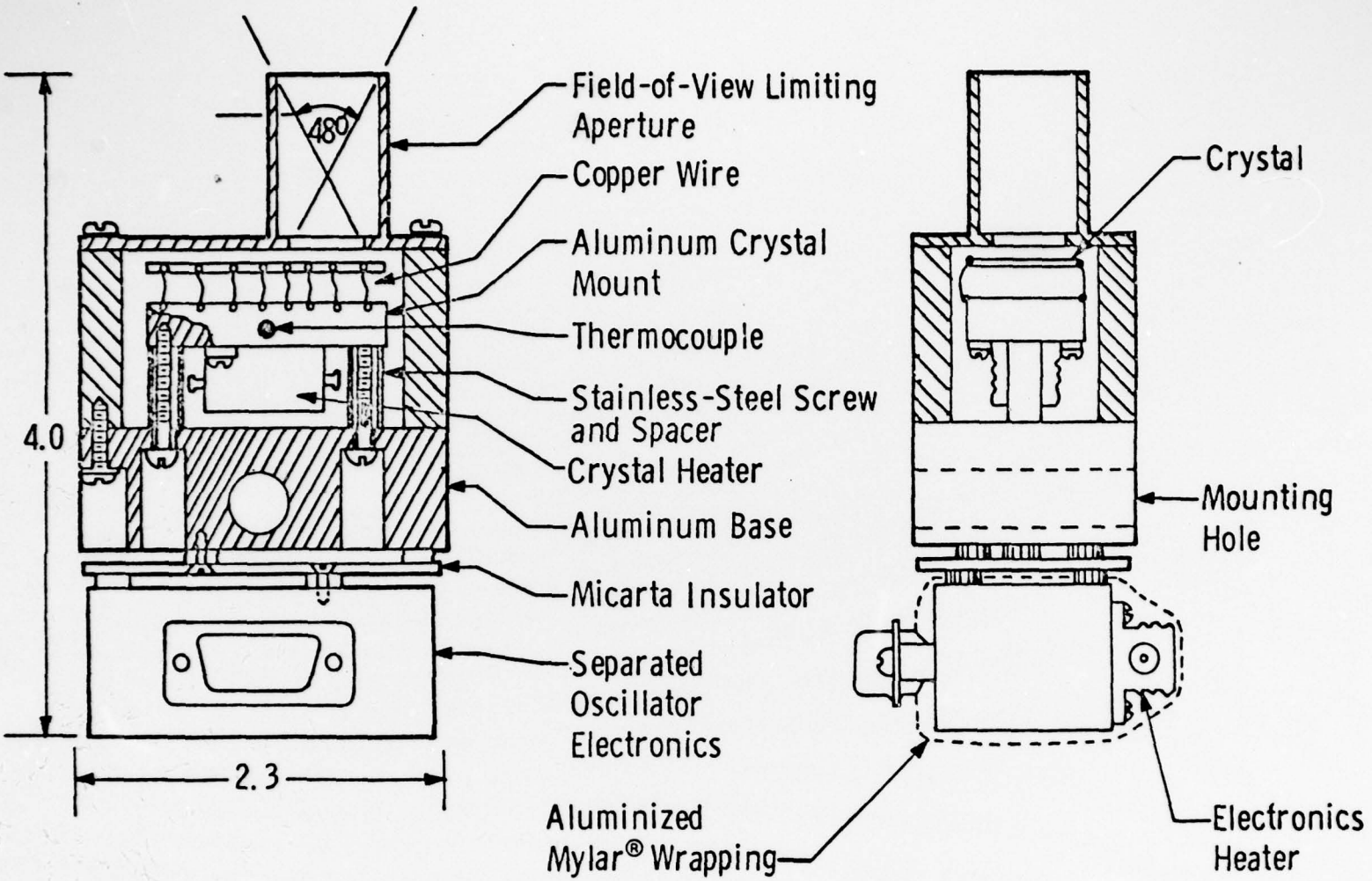

QUARTZ CRYSTAL MICROBALANCE

Figure 3

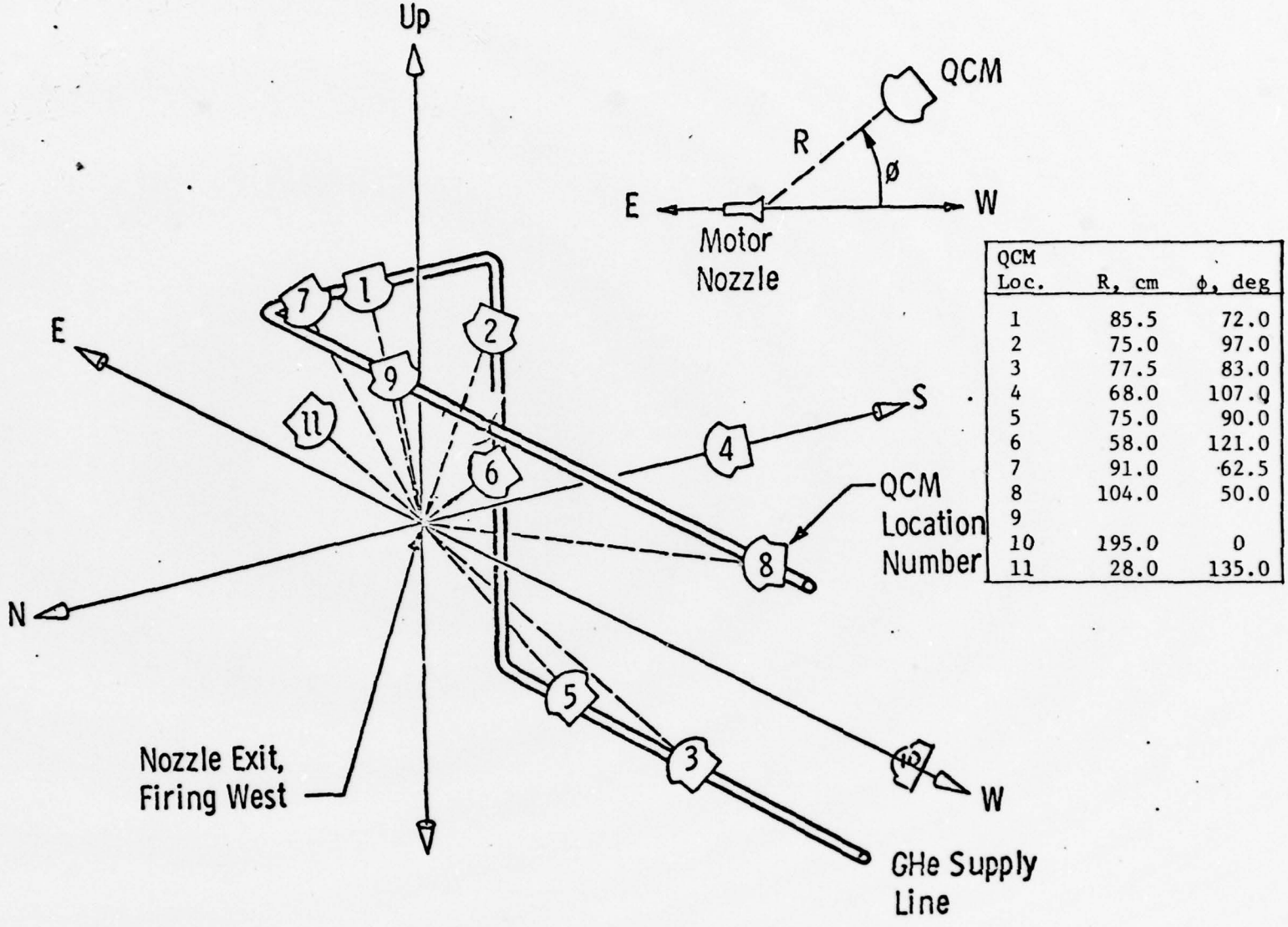

QCM Loc.	R, cm	ϕ, deg
1	85.5	72.0
2	75.0	97.0
3	77.5	83.0
4	68.0	107.0
5	75.0	90.0
6	58.0	121.0
7	91.0	62.5
8	104.0	50.0
9		
10	195.0	0
11	28.0	135.0

TYPICAL QCM LOCATIONS IN 10V CHAMBER

FIG. 4

10V CHAMBER

SIDE VIEW

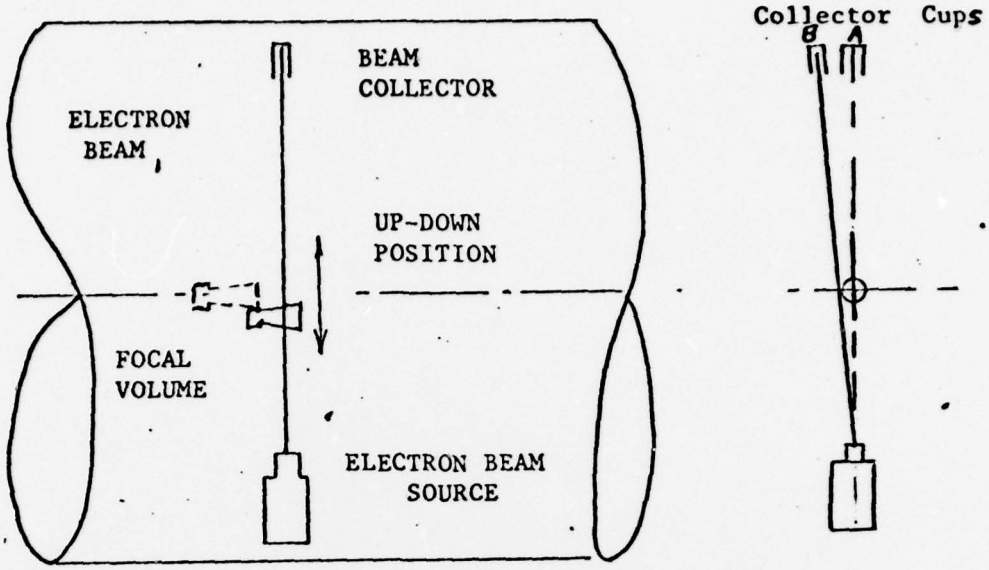

---------Forward Flow Measurements
————————Back Flow Measurements

TOP VIEW

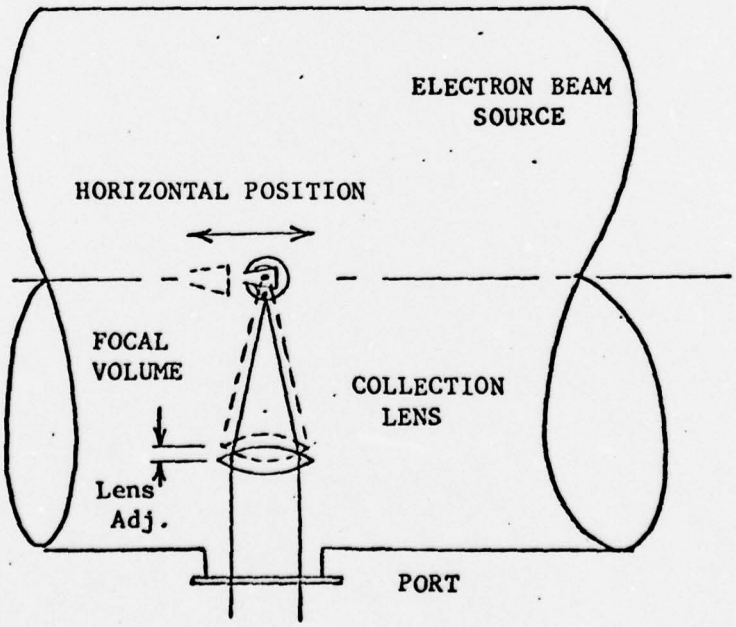

Fig. 5 10V BIPROP ELECTRON BEAM MEASUREMENTS FOR BACKFLOW AND FORWARD FLOW STUDIES

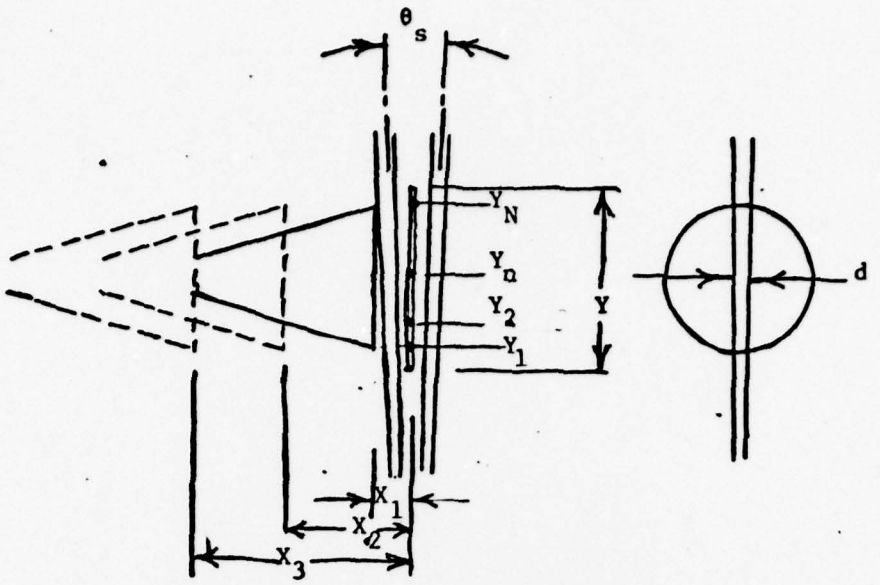

(a) Forward Flow Region

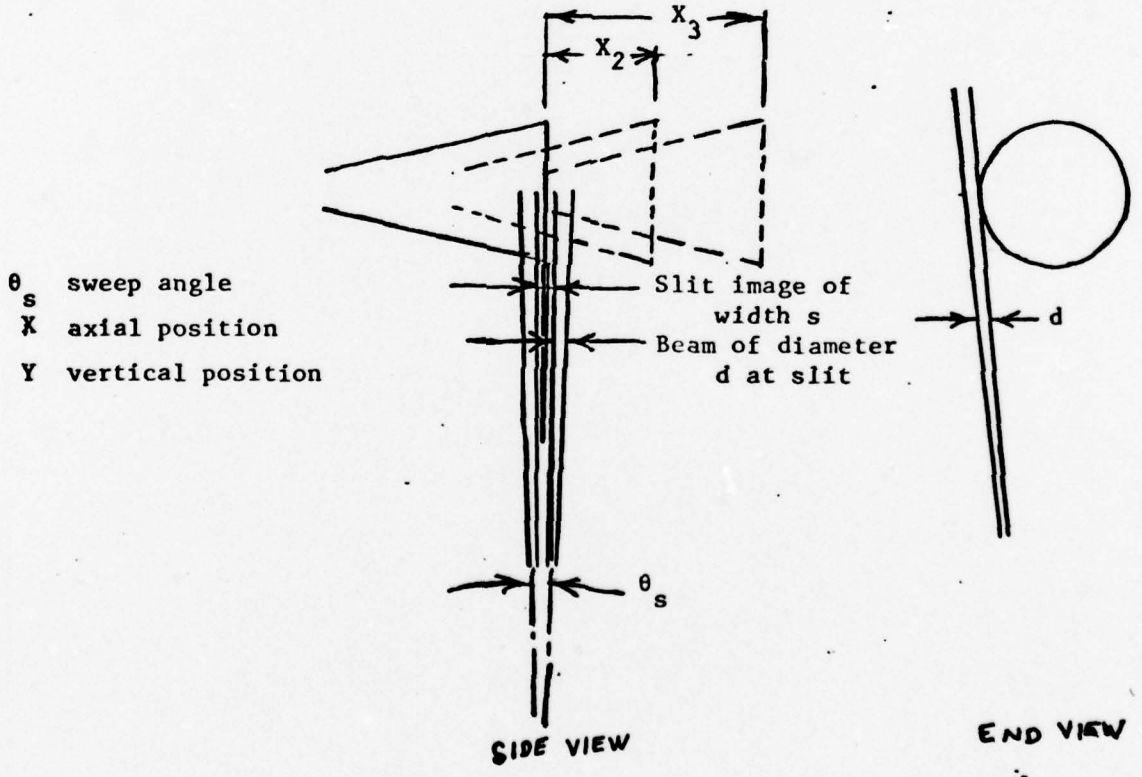

(b) Backflow Region

Fig. 6 FLOW FIELD MAPPING TECHNIQUE

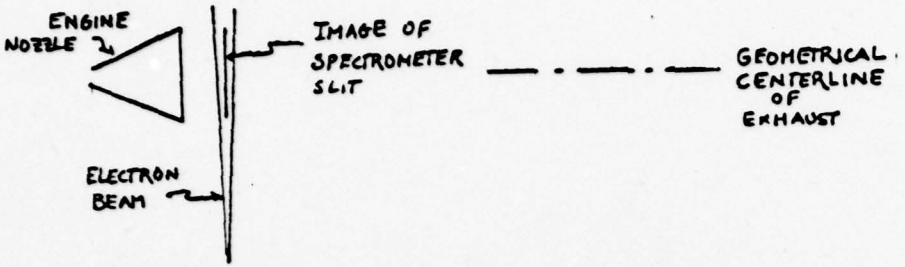

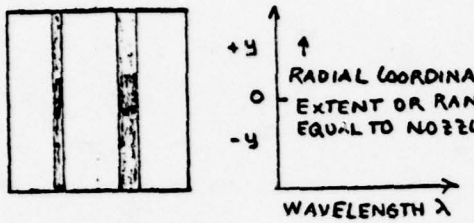

APPEARANCE OF INTENSIFIER OUTPUT FOR ONLY TWO MOLECULAR BAND SYSTEMS

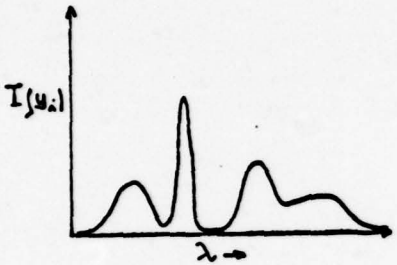

VARIATION OF INTENSIFIER OUTPUT WITH WAVELENGTH OR ABSCISSA AT FIXED RADIAL POSITION

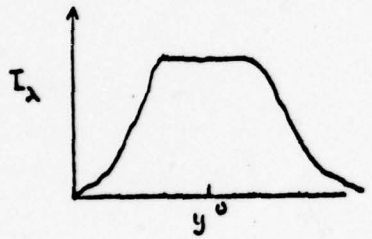

VARIATION OF INTENSIFIER OUTPUT WITH RADIAL POSITION AT FIXED WAVELENGTH λ

Fig. 7 INTENSIFIER APPLICATION

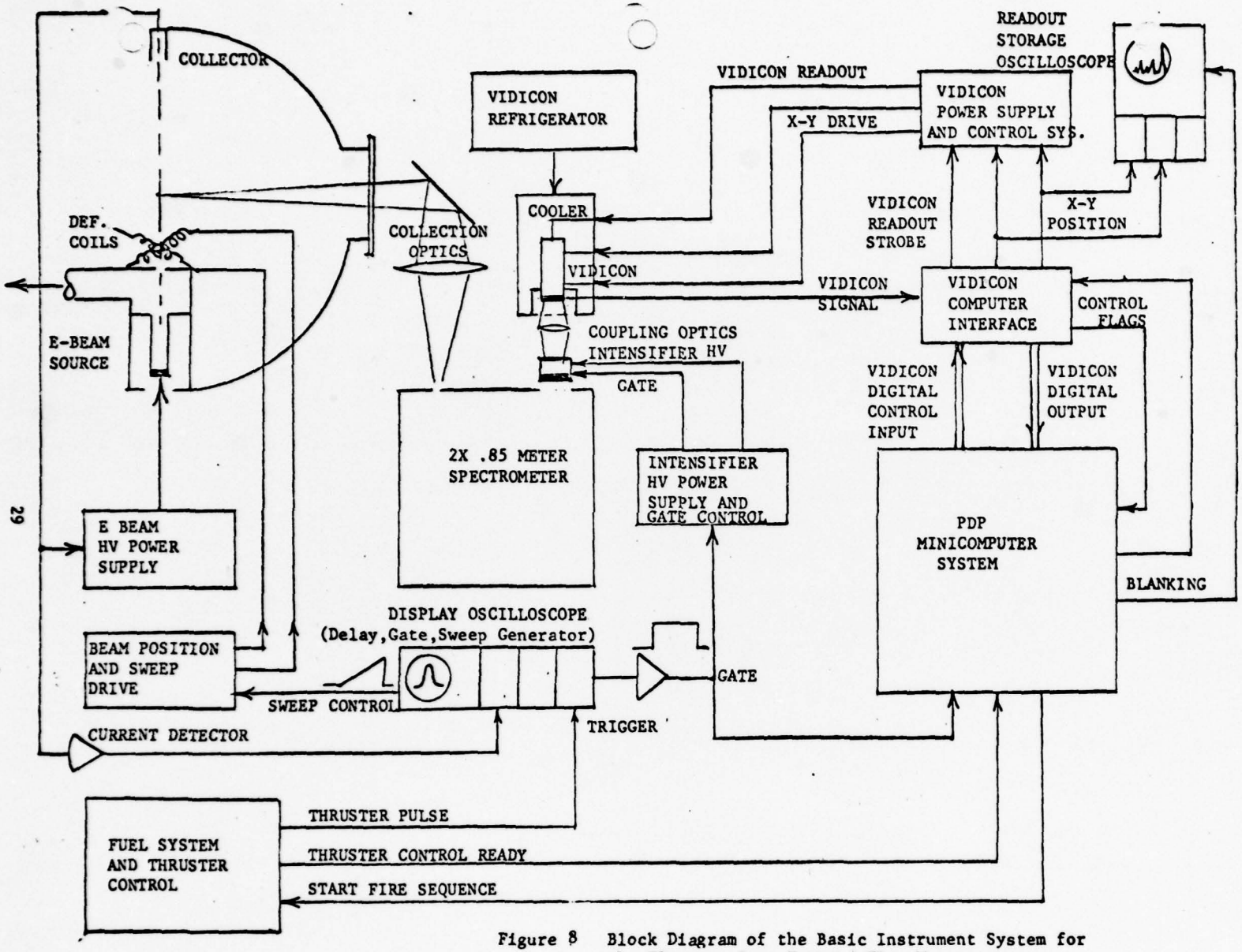

Figure 8 Block Diagram of the Basic Instrument System for the Electron Beam Forward Flow Measurements.

Figure 9 Block Diagram of Spectrometer Detector System for Electron Beam PMT Measurements.

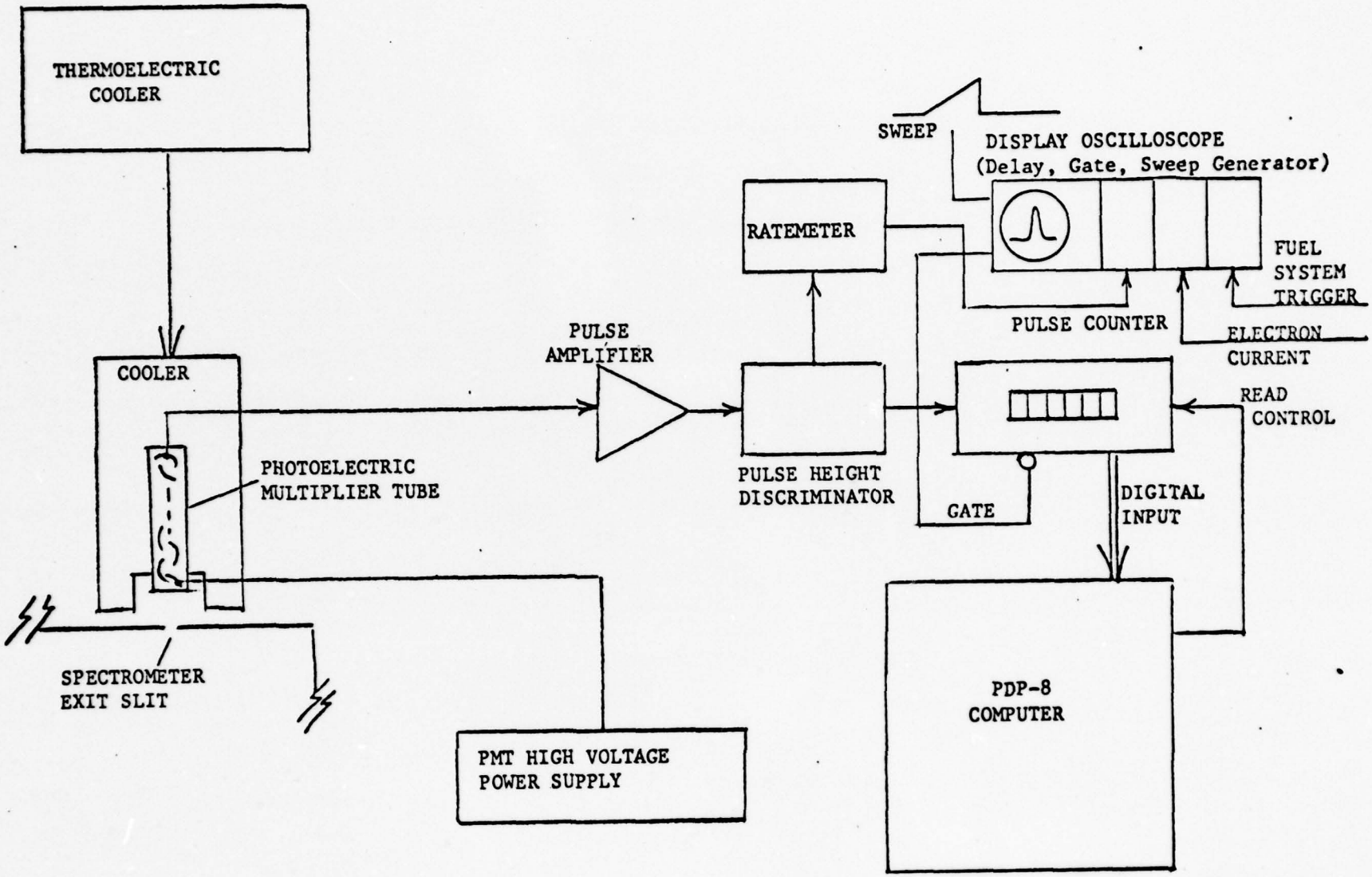

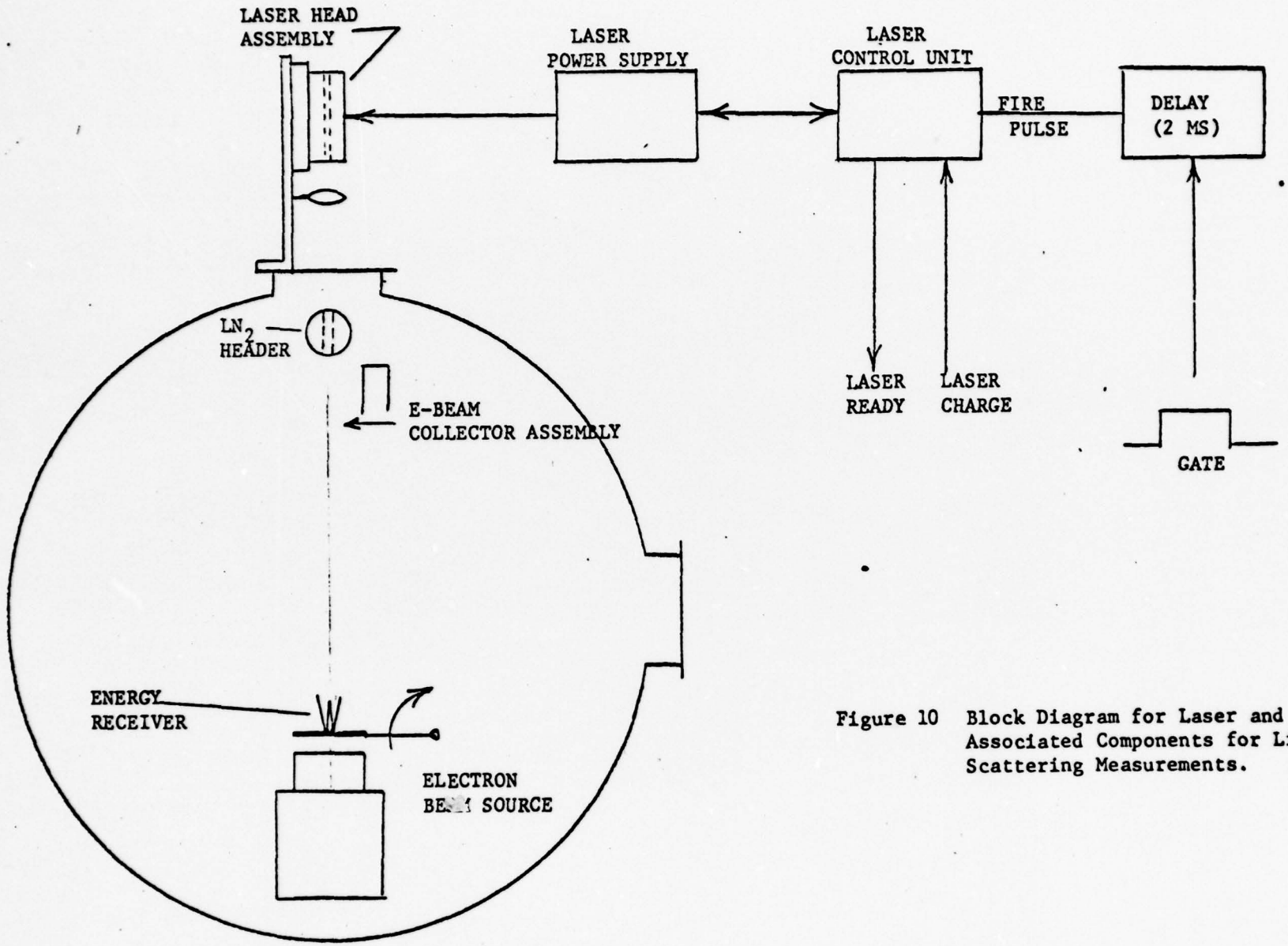

Figure 10 Block Diagram for Laser and Associated Components for Light Scattering Measurements.

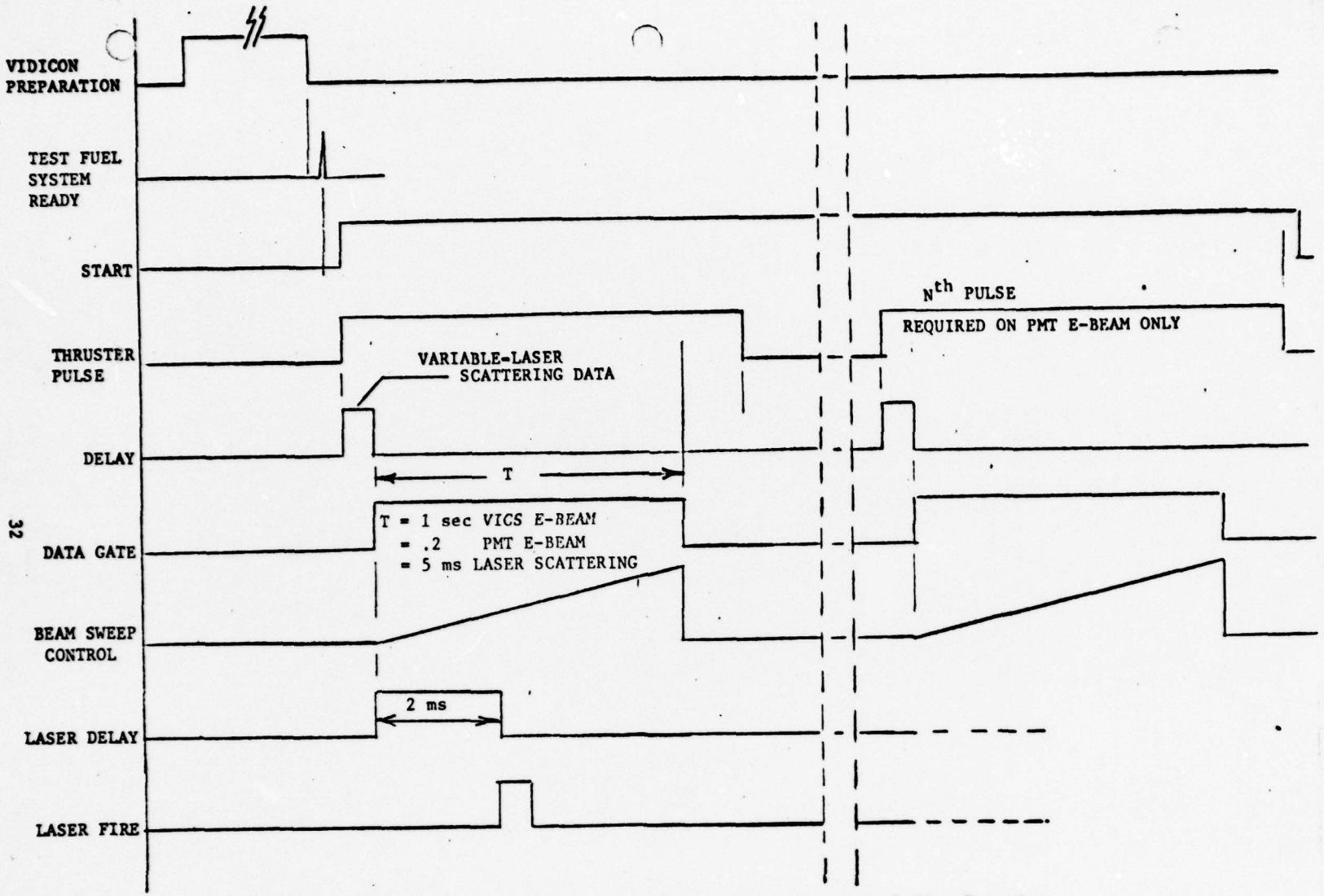

Figure 11 Timing Diagram for Data Acquisition Sequence. Actual Time Duration Depends Upon Specific Experiment Involved.

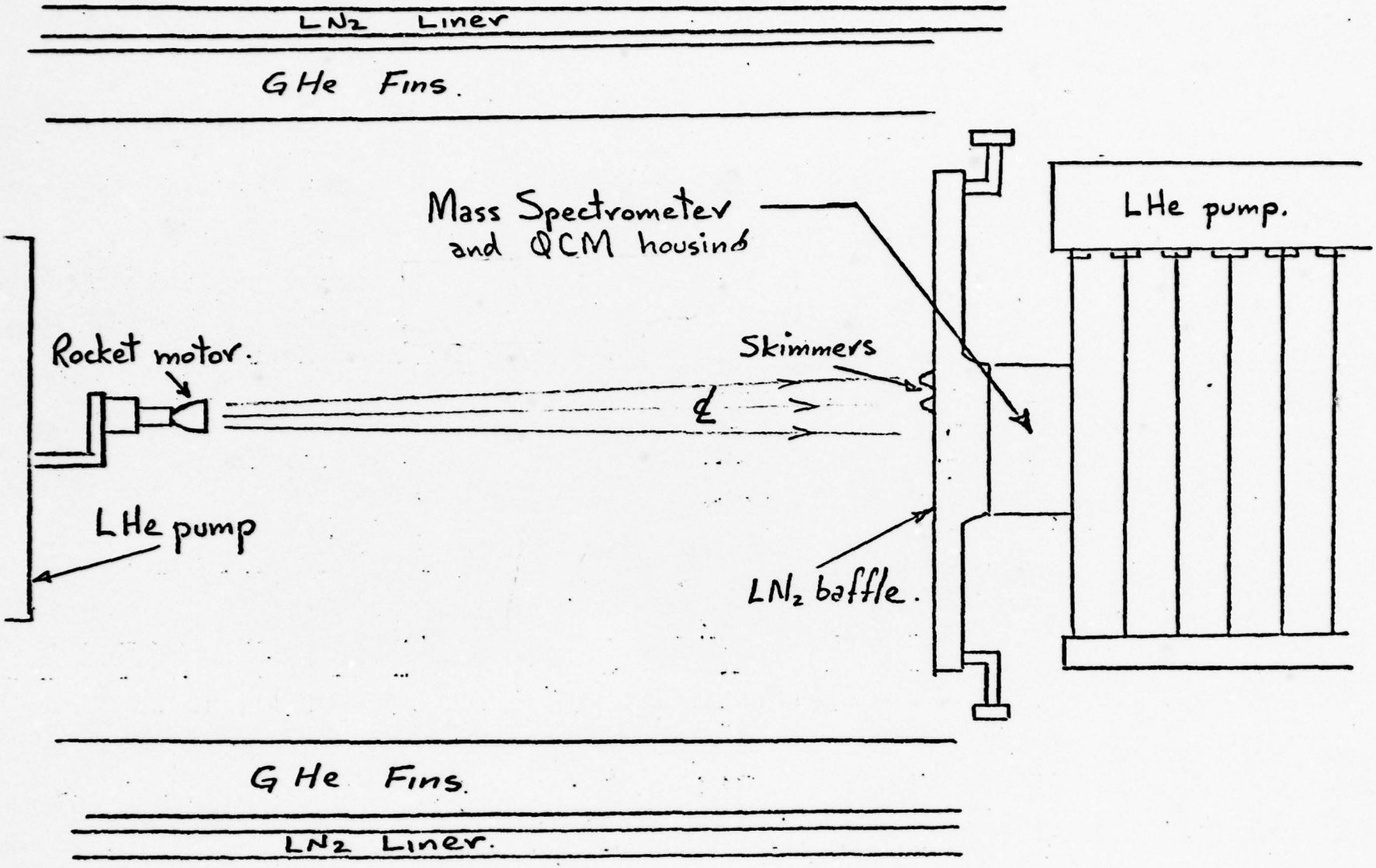

Fig. 12 Mass Spectrometer Installation

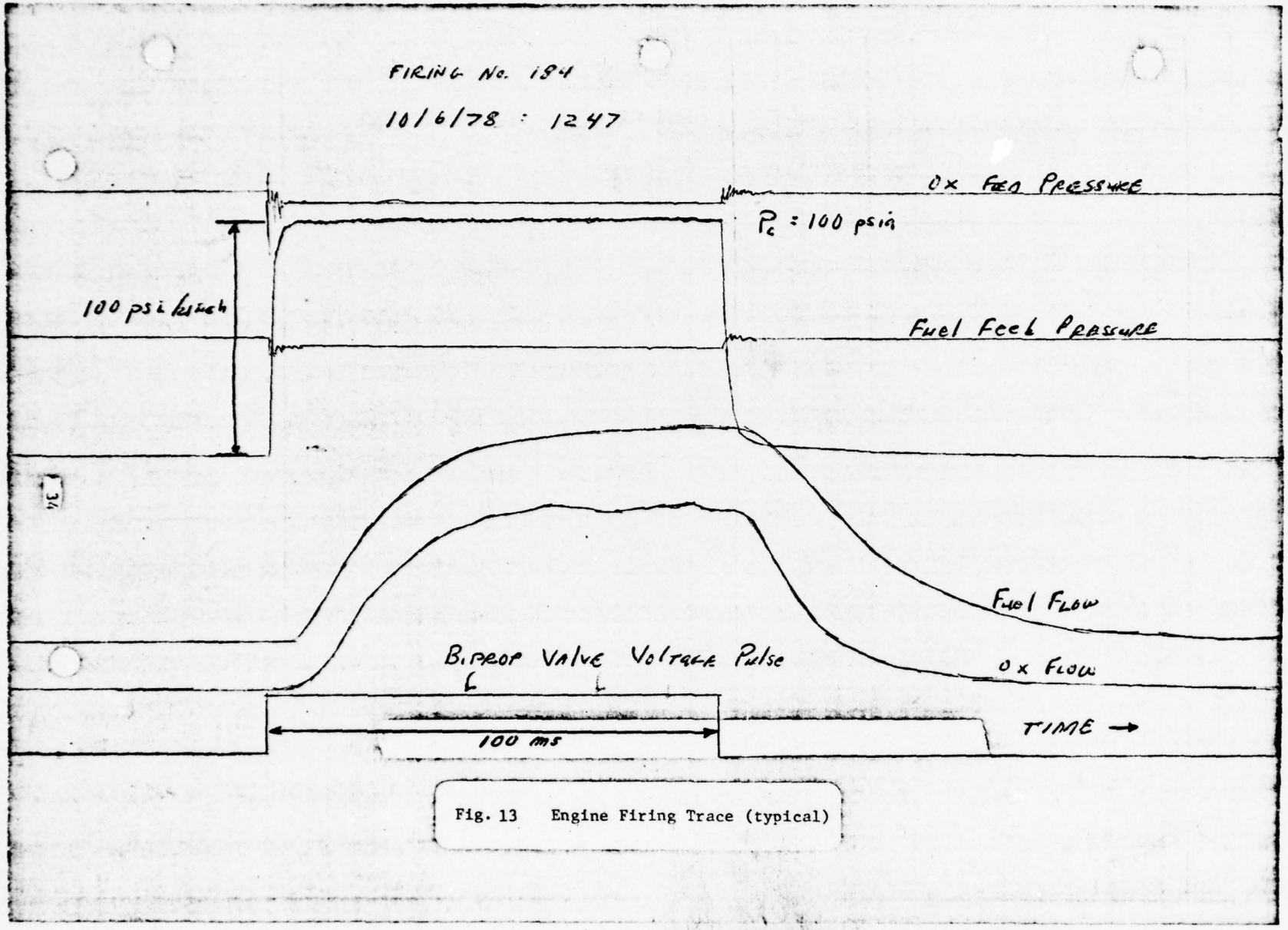

Fig. 13 Engine Firing Trace (typical)

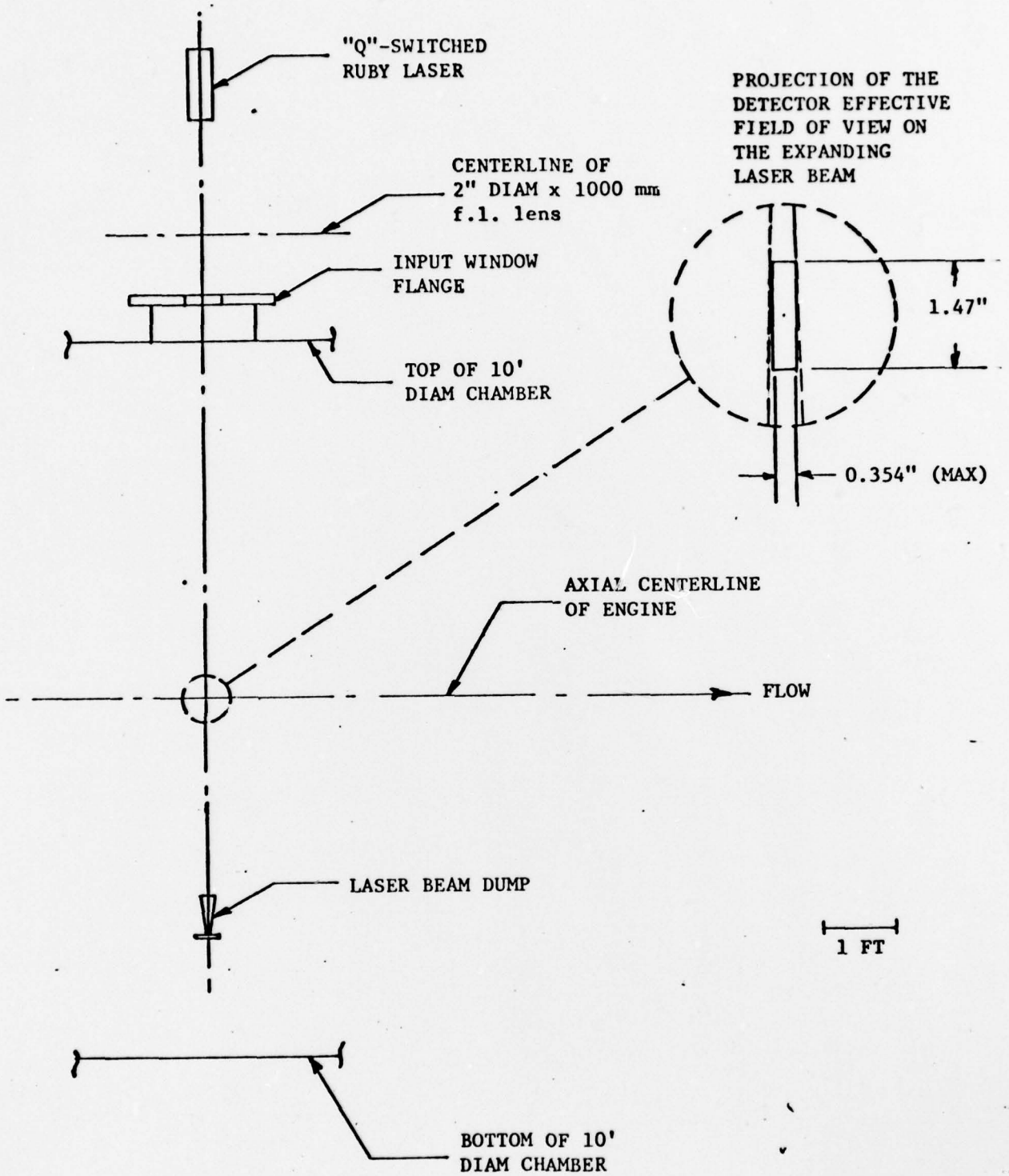

Fig. 14
LASER BEAM INJECTION SCHEME

SCHEMATIC DIAGRAM

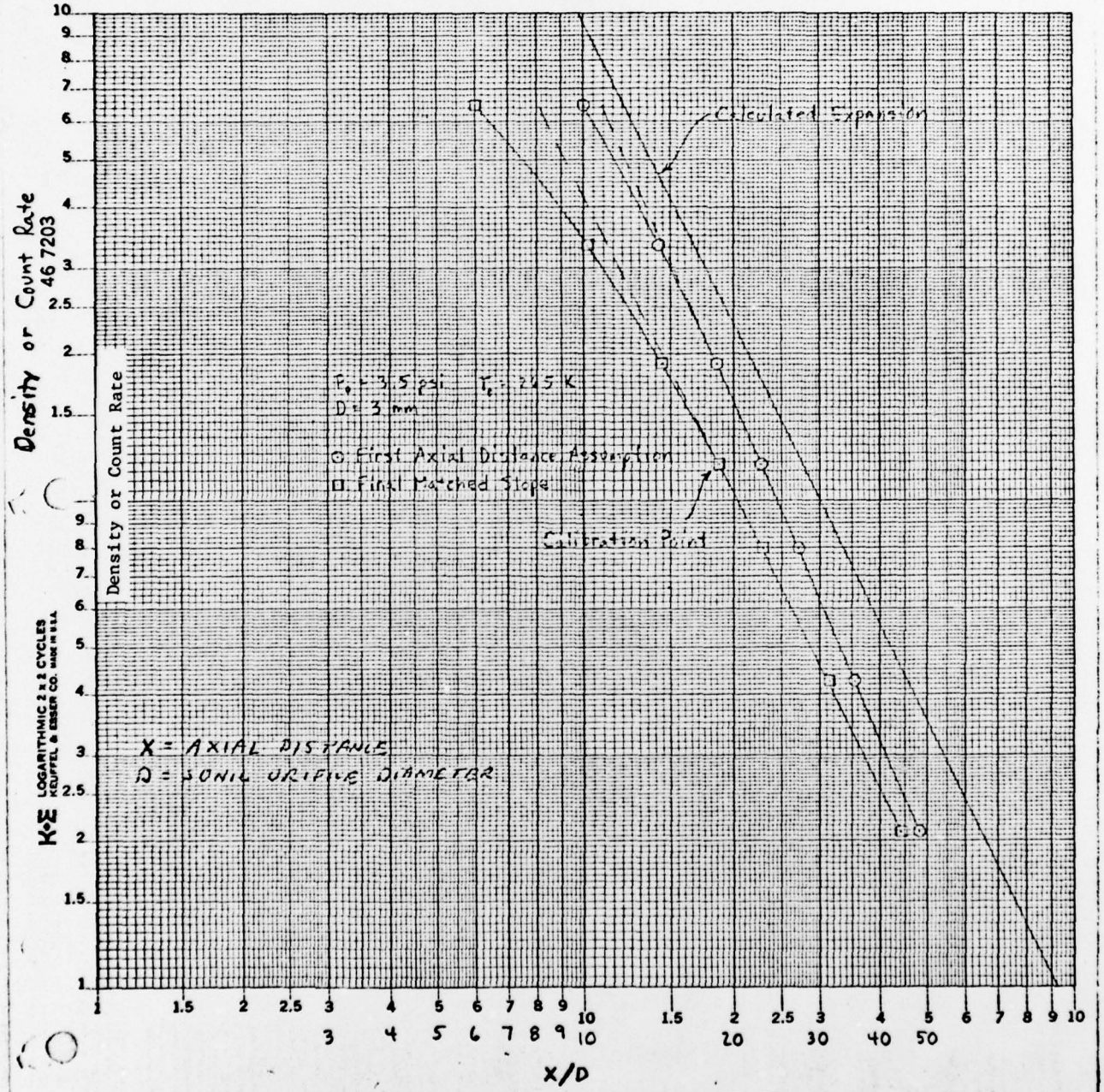

Fig. 15 Sonic Orifice Axial Scan

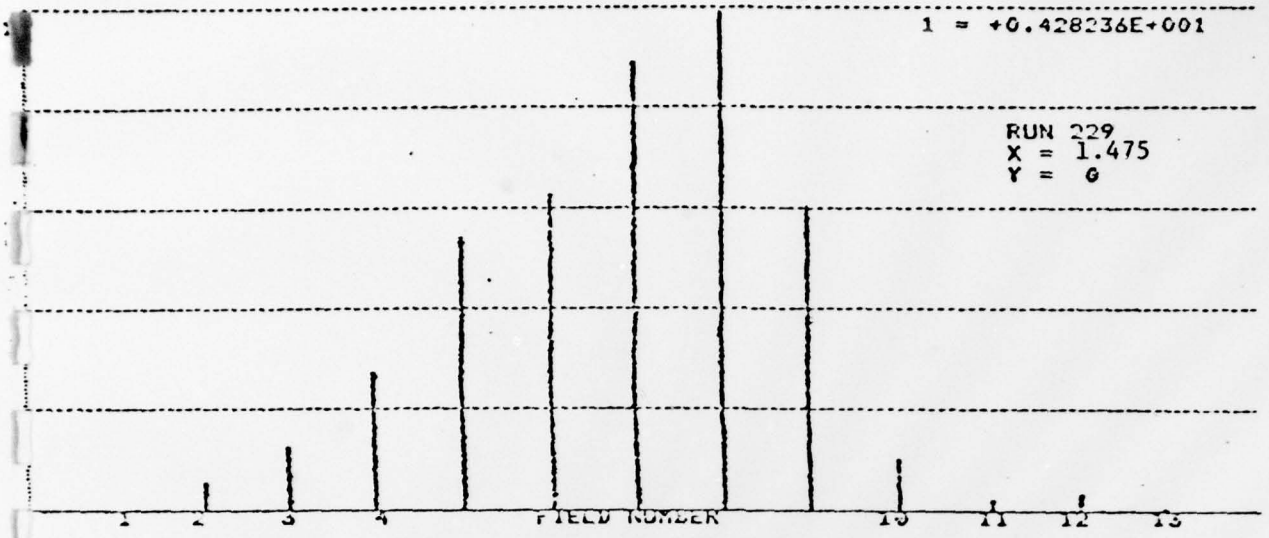

Figure 16 Normalized Radial Profile at Noted Position for Electron Beam Forward Flow Using Optical System I.

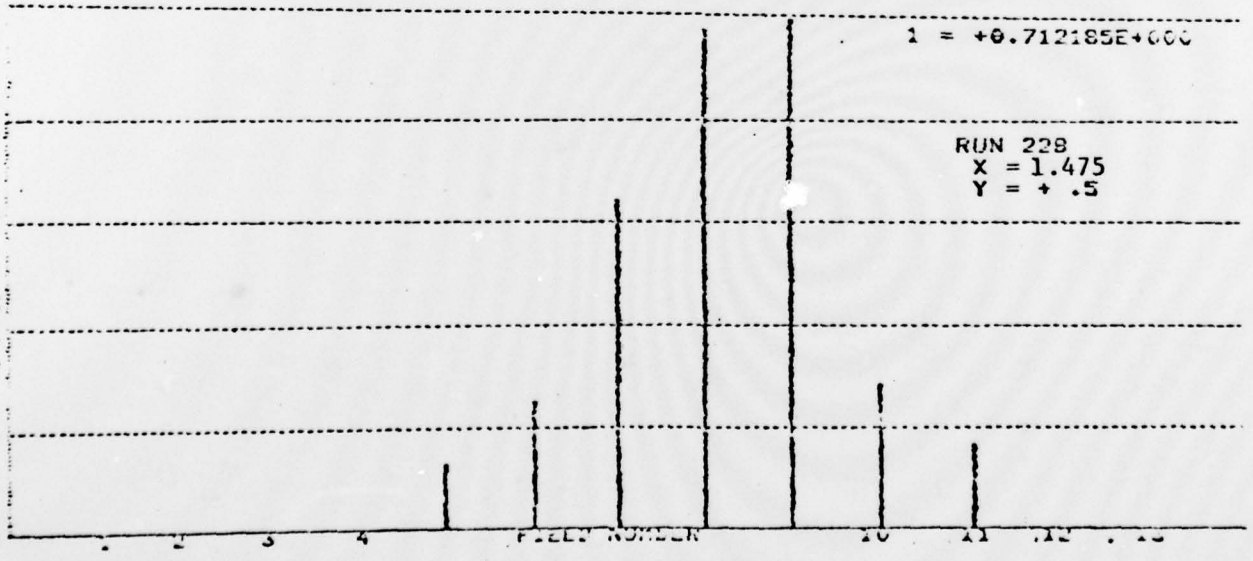

Figure 17 Normalized Off-axis Profile at Noted Position for Electron Beam Forward Flow Using Optical System I.

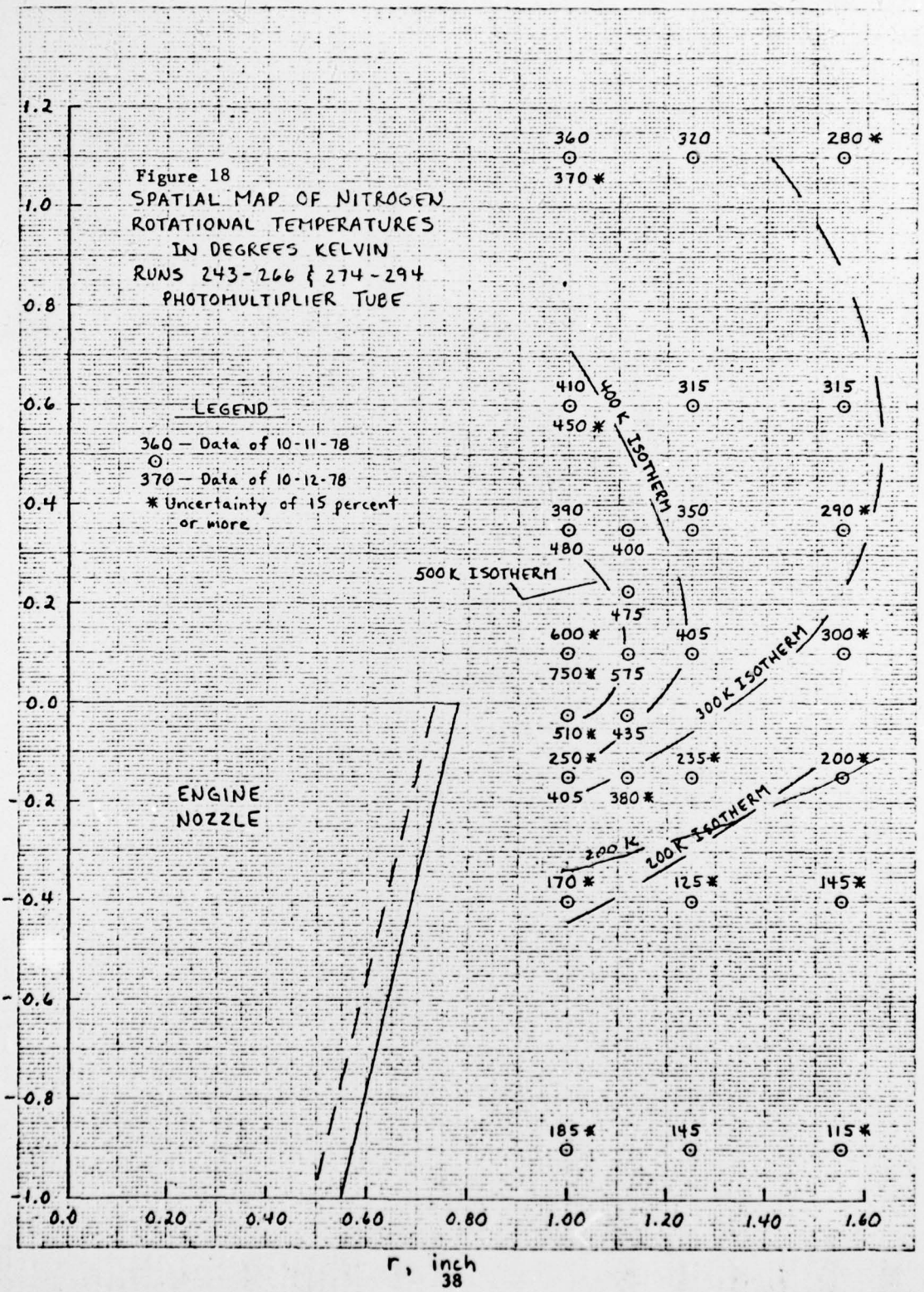
Figure 18
SPATIAL MAP OF NITROGEN ROTATIONAL TEMPERATURES IN DEGREES KELVIN
RUNS 243-266 & 274-294
PHOTOMULTIPLIER TUBE
LEGEND
360 — Data of 10-11-78
370 — Data of 10-12-78
* Uncertainty of 15 percent or more
ENGINE NOZZLE
400 K ISOTHERM
500 K ISOTHERM
300 K ISOTHERM
200 K
200 K ISOTHERM
X, inch
r, inch
1.2
1.0
0.8
0.6
0.4
0.2
0.0
-0.2
-0.4
-0.6
-0.8
-1.0
0.0
0.20
0.40
0.60
0.80
1.00
1.20
1.40
1.60
360
370
320
280
410
450
315
315
390
480
350
290
400
500
475
600
750
405
300
575
510
435
250
405
235
380
200
170
125
145
185
145
115

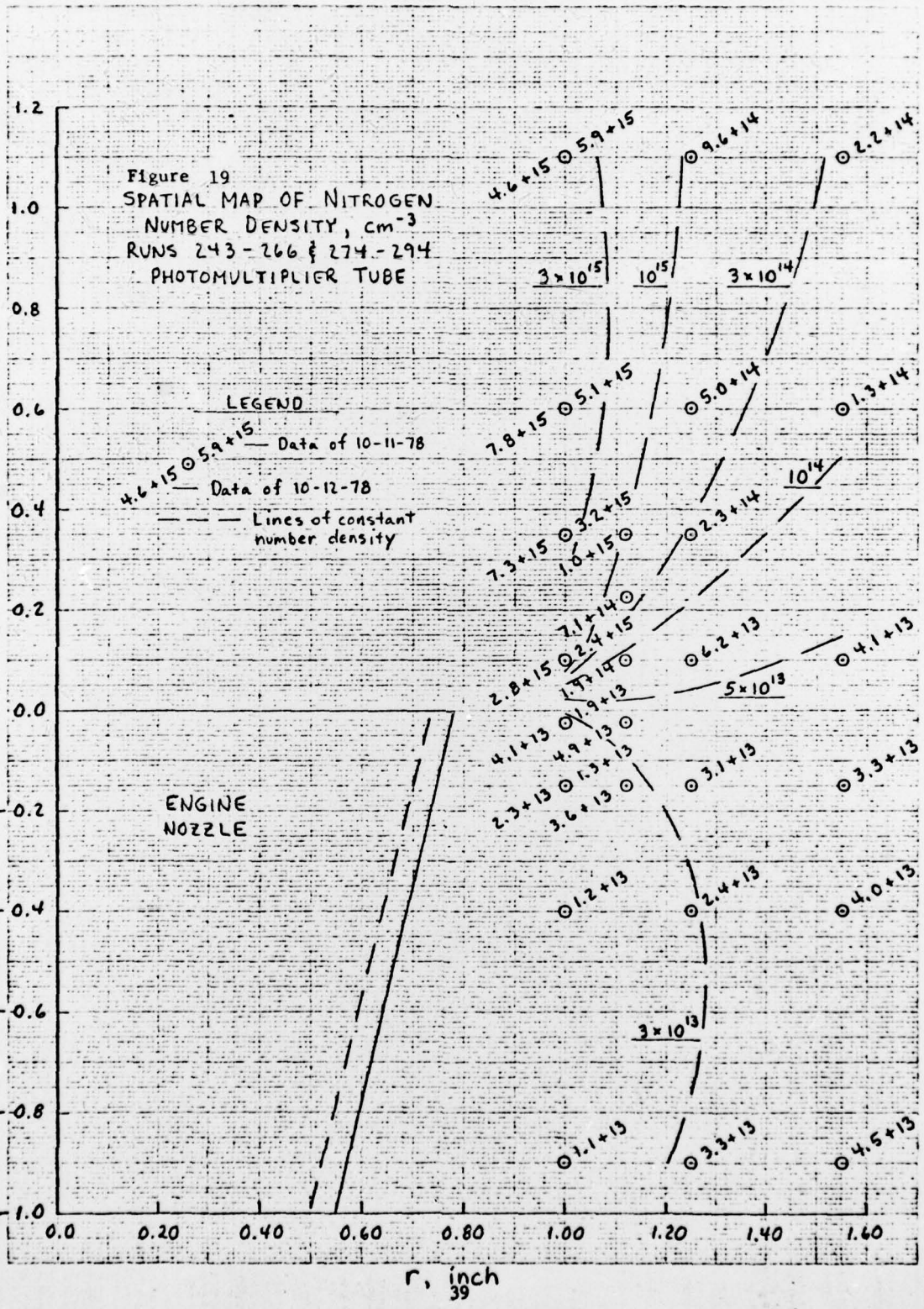
Figure 19
SPATIAL MAP OF NITROGEN NUMBER DENSITY, cm⁻³
RUNS 243-266 & 274-294
PHOTOMULTIPLIER TUBE
LEGEND
— Data of 10-11-78
— Data of 10-12-78
— — — Lines of constant number density
ENGINE NOZZLE
X, inch
r, inch
1.2
1.0
0.8
0.6
0.4
0.2
0.0
-0.2
-0.4
-0.6
-0.8
-1.0
0.0
0.20
0.40
0.60
0.80
1.00
1.20
1.40
1.60
4.6+15
5.9+15
9.6+14
2.2+14
3×10¹⁵
10¹⁵
3×10¹⁴
7.8+15
5.1+15
5.0+14
1.3+14
10¹⁴
7.3+15
3.2+15
2.3+14
1.0+15
7.1+14
2.8+15
2.4+15
1.4+14
6.2+13
4.1+13
5×10¹³
4.1+13
1.9+13
4.9+13
1.3+13
3.1+13
3.3+13
2.3+13
3.6+13
1.2+13
2.4+13
4.0+13
3×10¹³
1.1+13
3.3+13
4.5+13

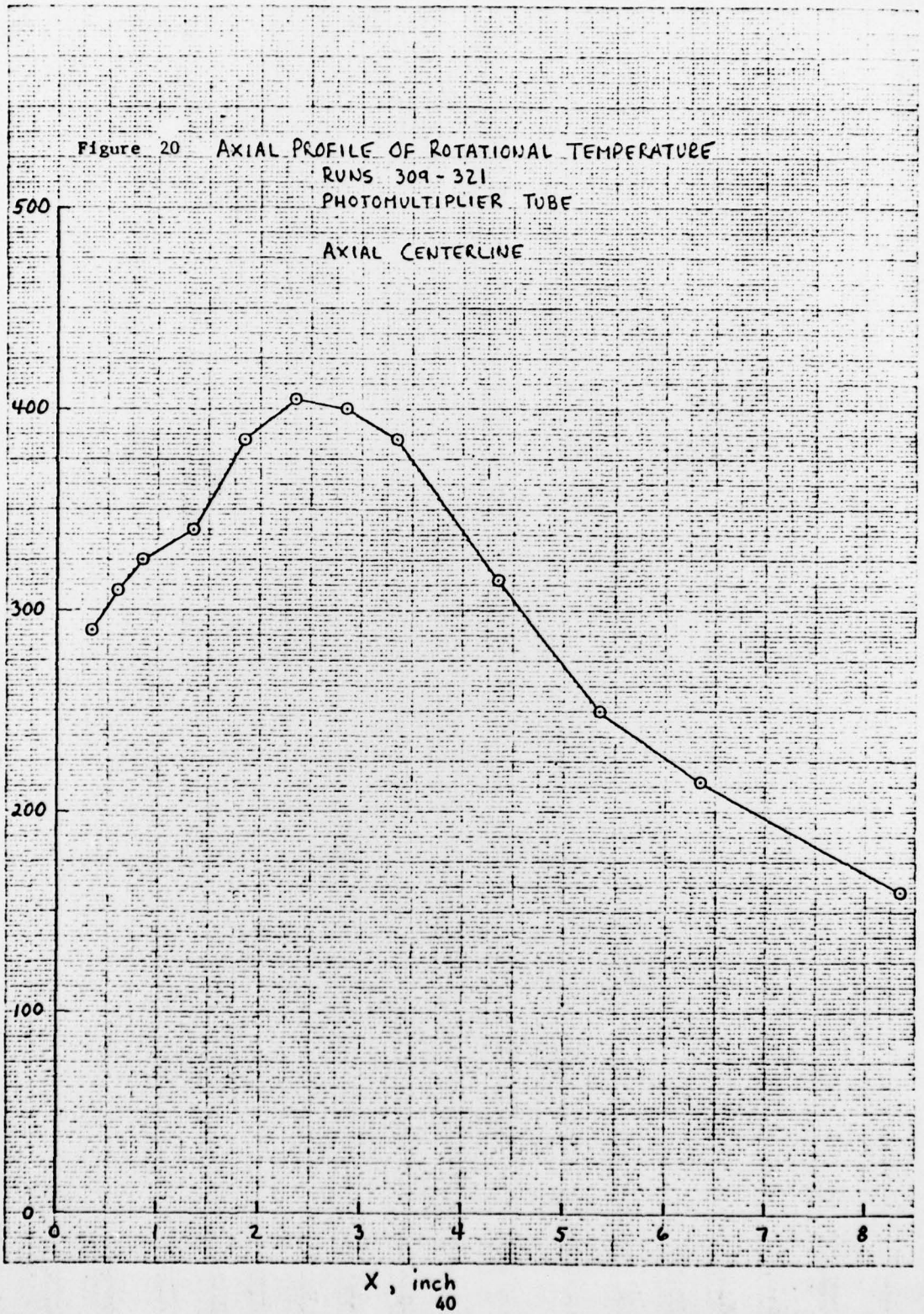
AXIAL PROFILE OF ROTATIONAL TEMPERATURE
RUNS 309 - 321
PHOTOMULTIPLIER TUBE
AXIAL CENTERLINE
500
400
300
200
100
0
T_R, KELVIN
0
1
2
3
4
5
6
7
8
X, inch

Figure 20

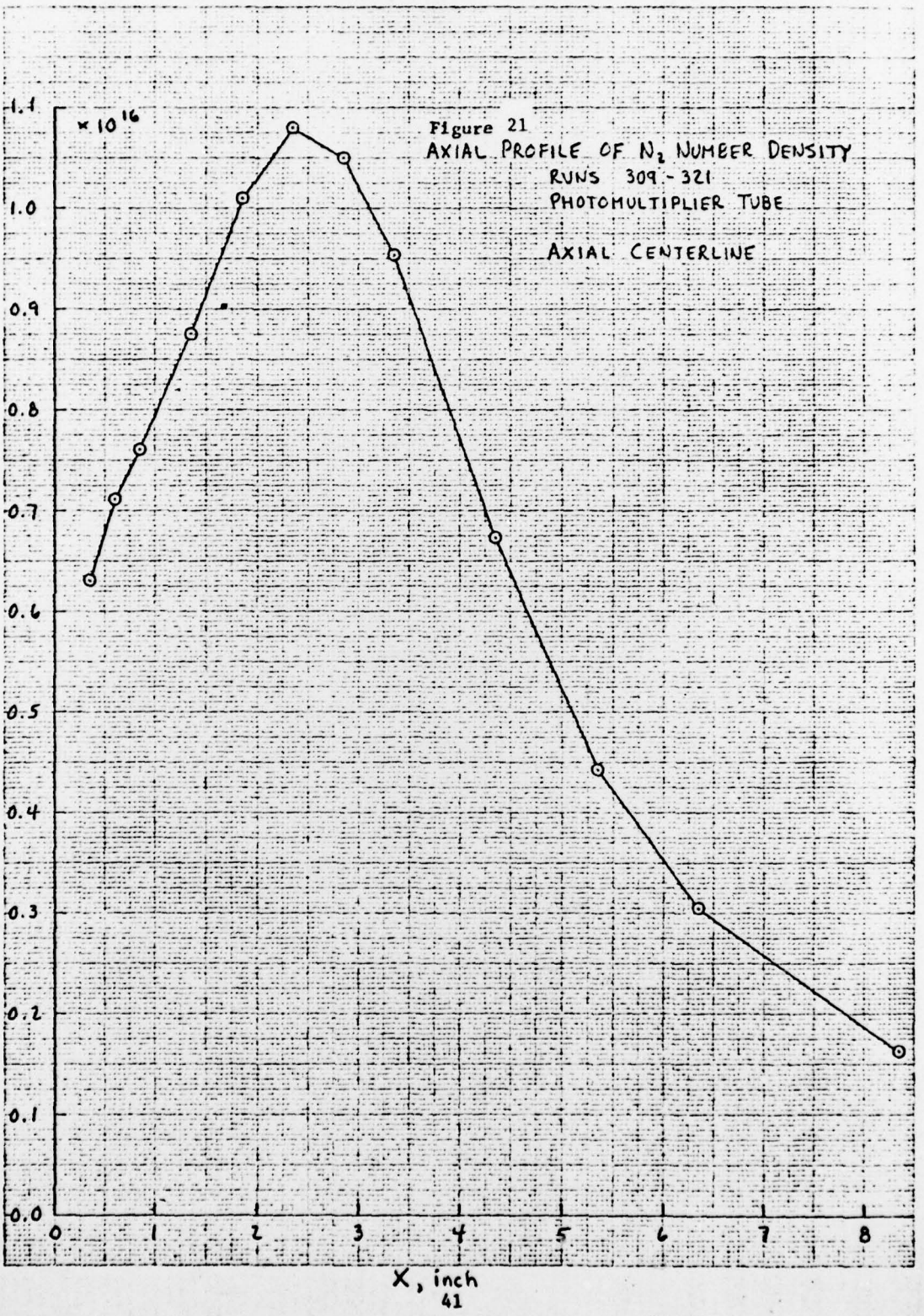
Figure 21
AXIAL PROFILE OF N_2 NUMBER DENSITY
RUNS 309 - 321
PHOTOMULTIPLIER TUBE
AXIAL CENTERLINE
× 10 16
1.1
1.0
0.9
0.8
0.7
0.6
0.5
0.4
0.3
0.2
0.1
0.0
N_2 NUMBER DENSITY, cm^{-3}
0
1
2
3
4
5
6
7
8
X, inch

Figure 22. RADIAL PROFILES OF ROTATIONAL TEMPERATURE
RUNS 322-345
PHOTOMULTIPLIER TUBE

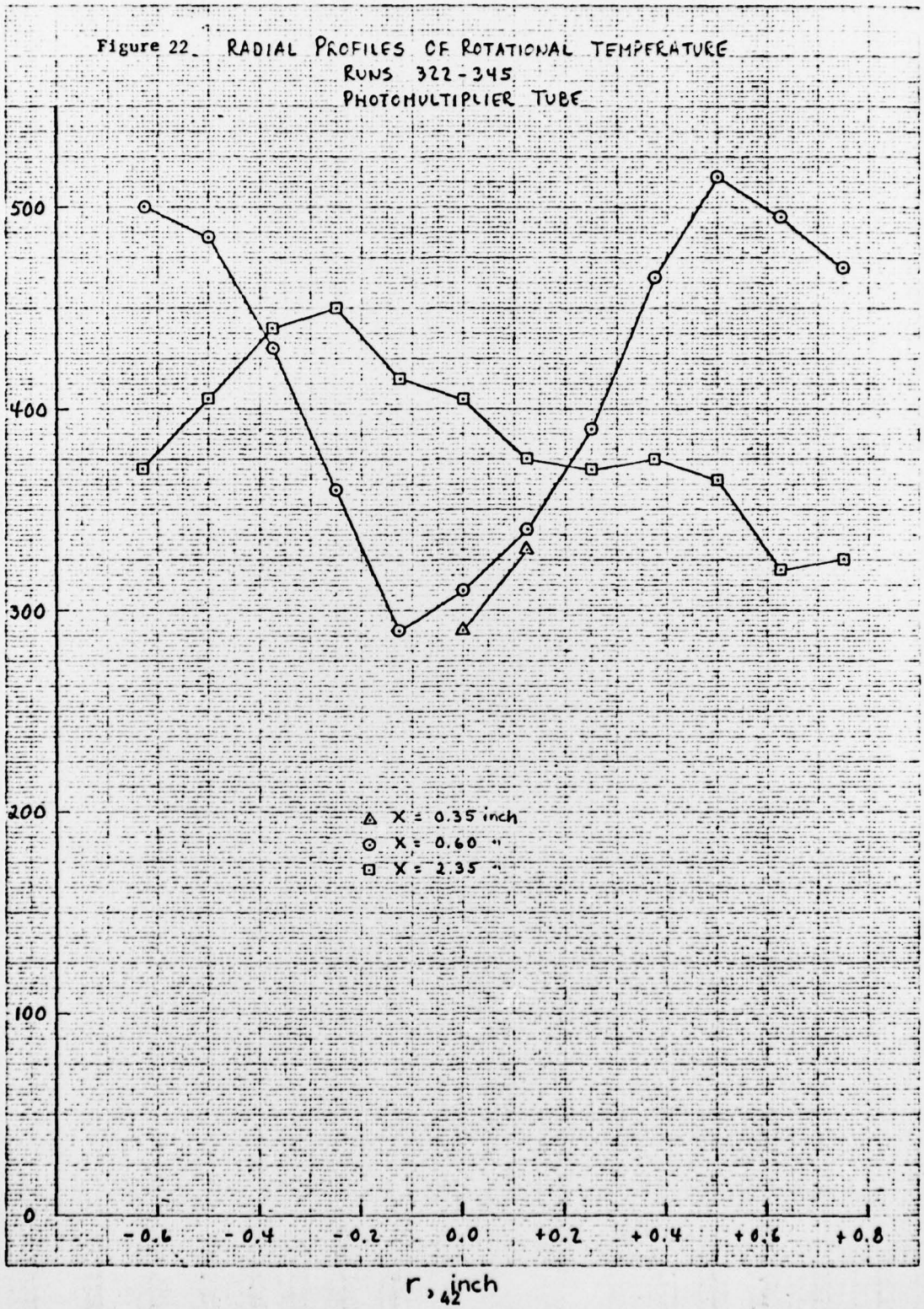

Figure 23 RADIAL PROFILES OF N_2 NUMBER DENSITY
RUNS 322 - 345
PHOTOMULTIPLIER TUBE

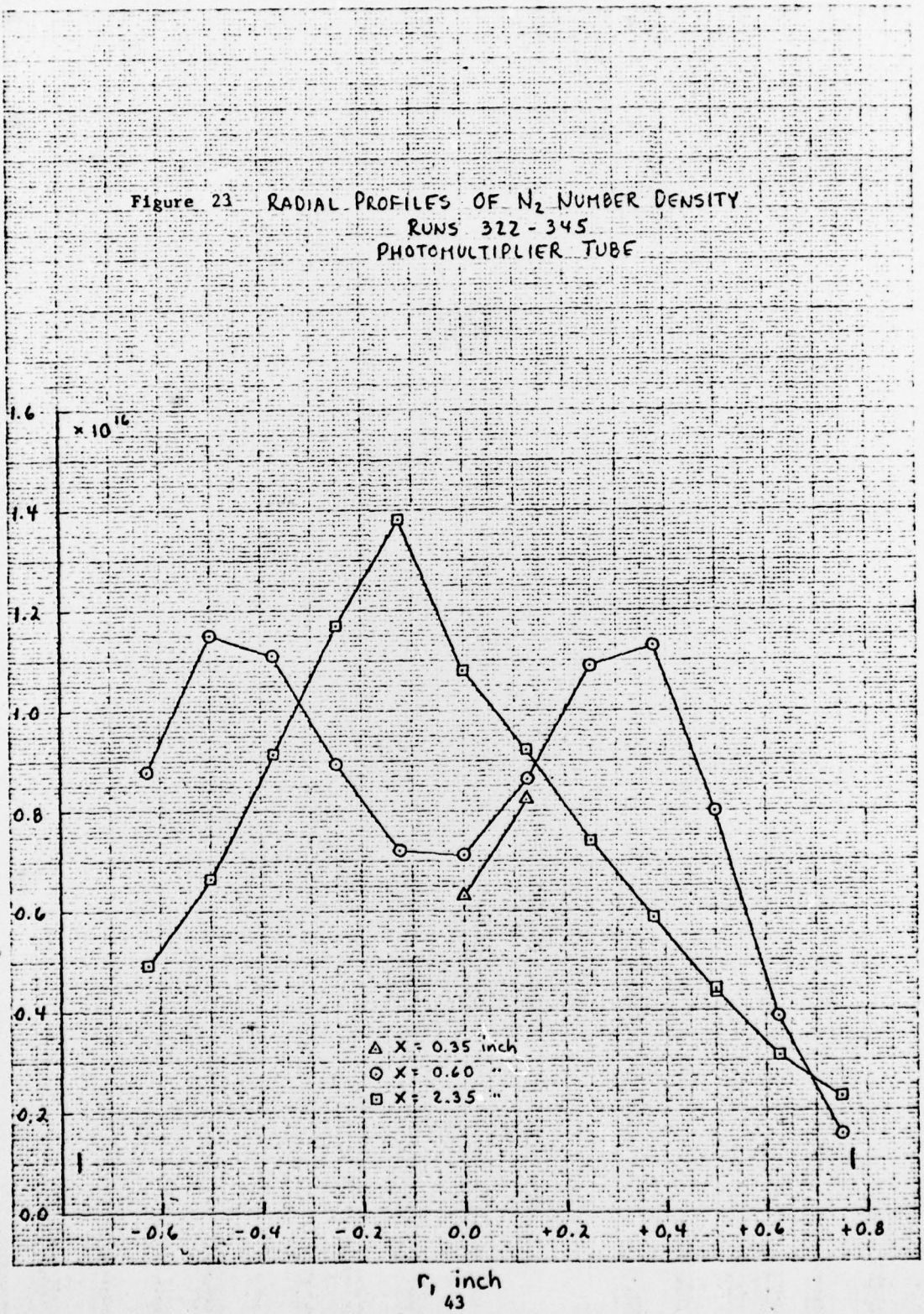

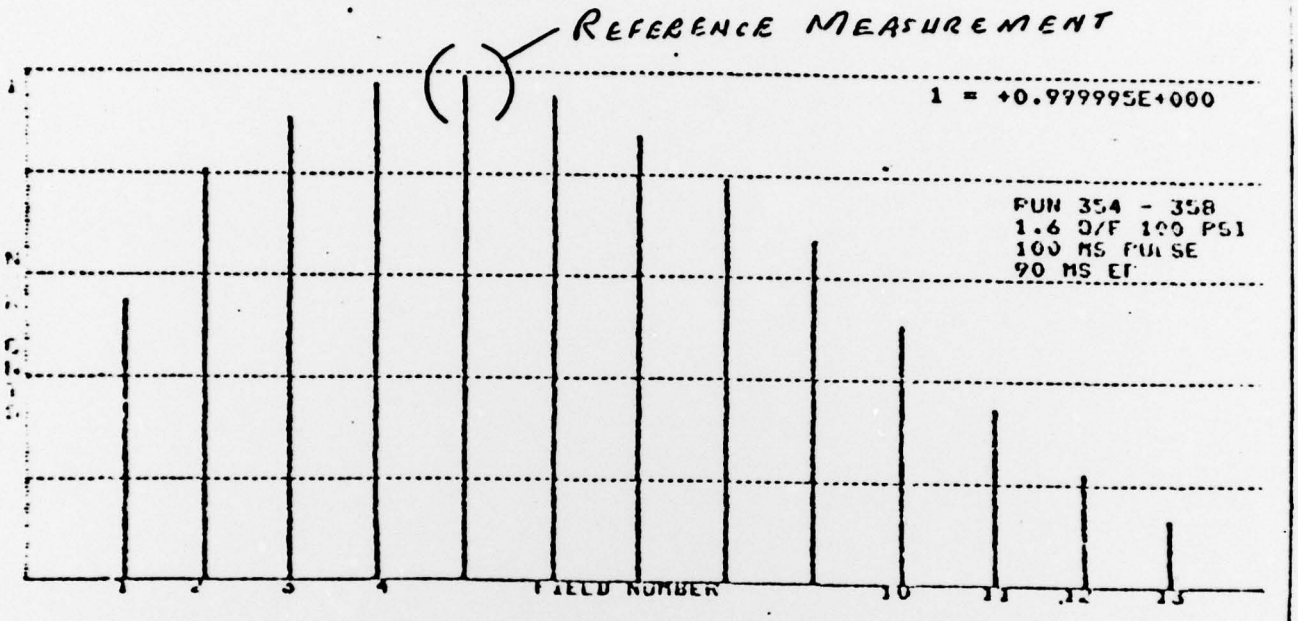

Figure 24 Radial Profile for Reference Data Taken for Light Scattering Measurements.

Figure 25 Composite Scattered Light Data for Runs 354 through 372 Showing Results for Fields 5 and 7 for Reference Pulse.

a. Time After Prop Valve Activation.

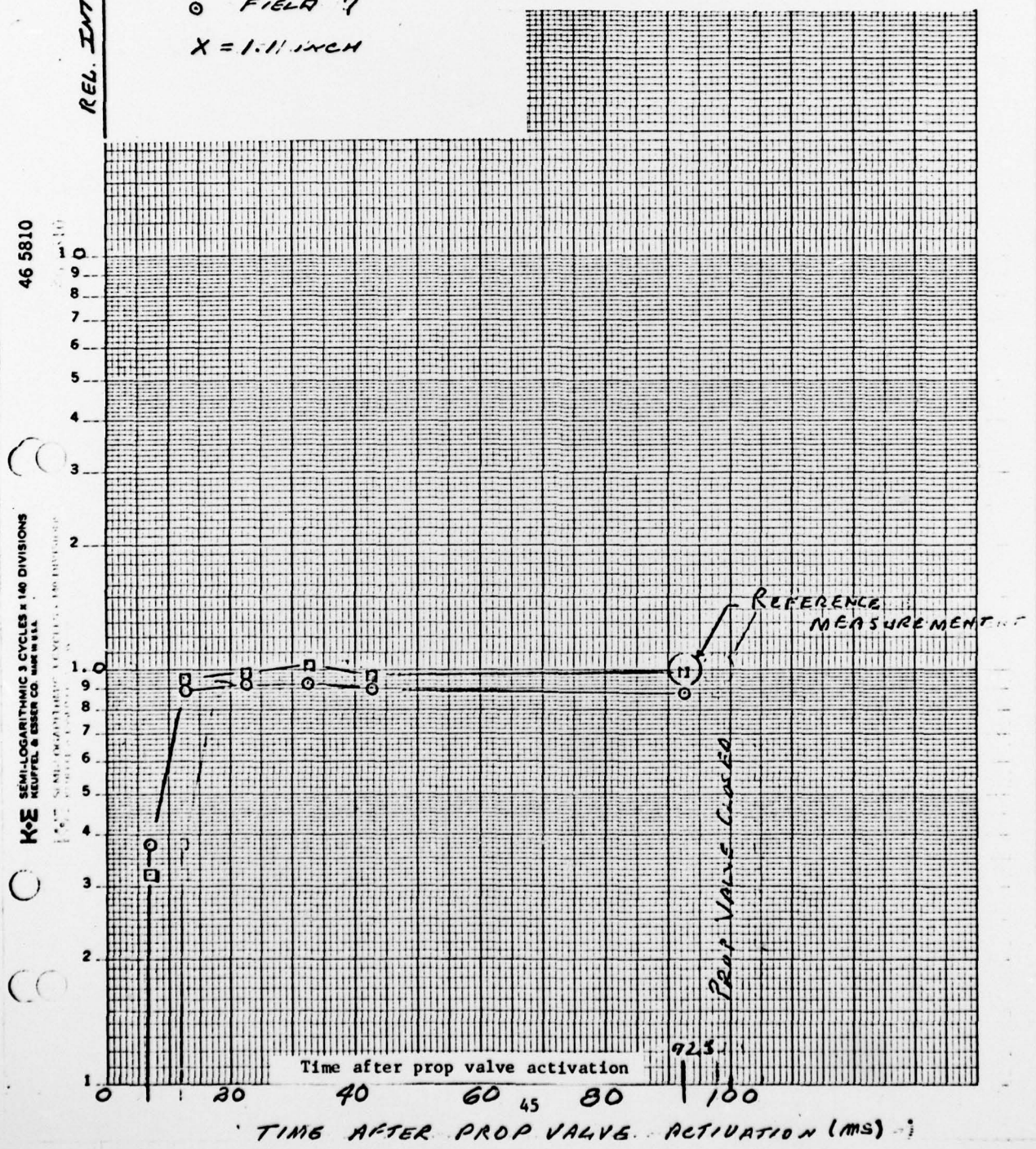

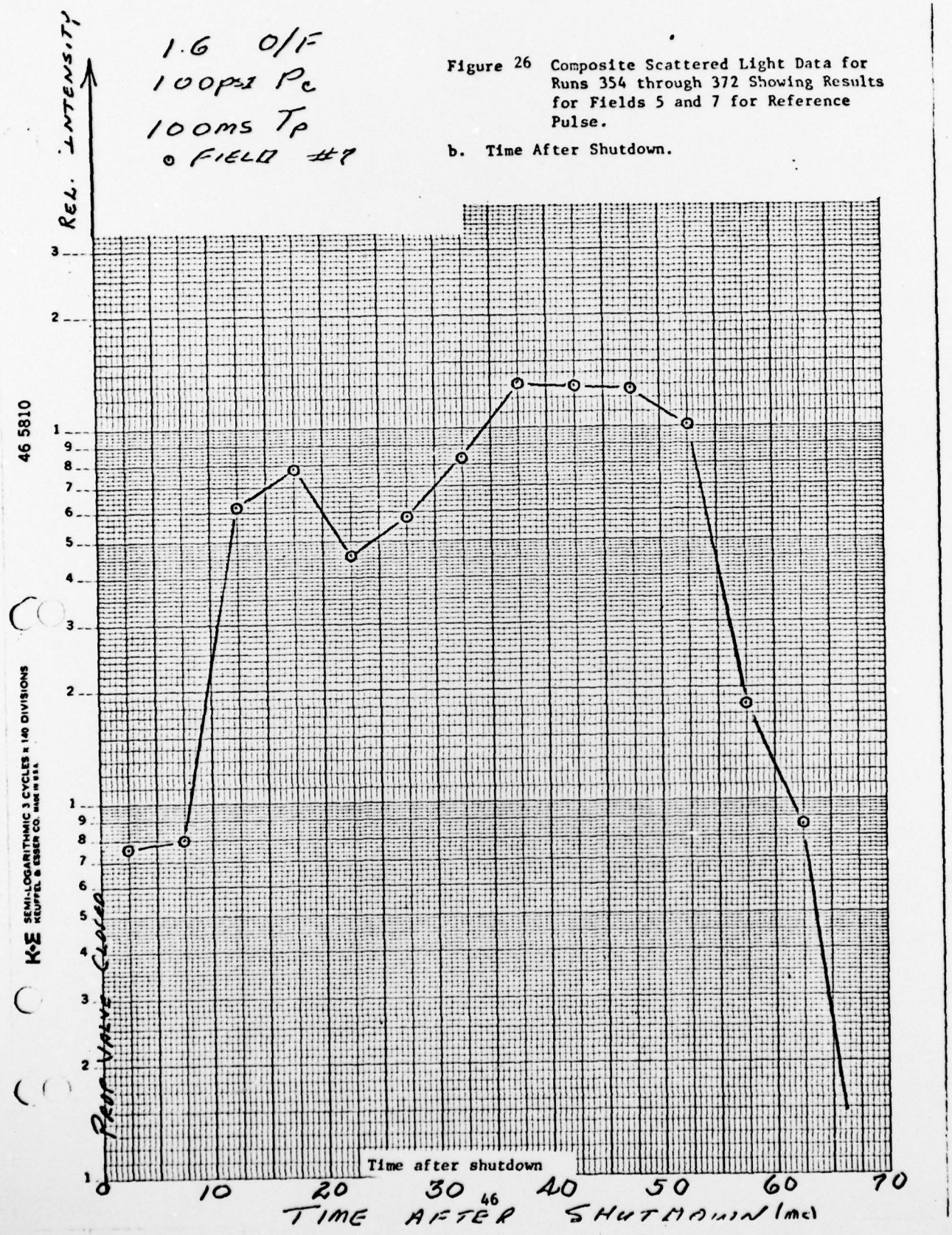

Figure 26 Composite Scattered Light Data for Runs 354 through 372 Showing Results for Fields 5 and 7 for Reference Pulse.

b. Time After Shutdown.

Table 1 Test Matrix Summary - Phase II Bipropellant Contamination Program

Date	Engine Firing	P_c(psia)	Pulse Width (ms)	O/F Ratio (nom)	Diagnostic Measurements
9/21	1-19	100	varied	1.6	Engine performance checkout.
9/21	20-54	100	1000	1.6	VICS checkout - forward flow.
9/22	55-80	100	250	1.6	Laser scattering measurement checkout.
10/3	81-168	100	1000	1.6	Forward flow N_2 number density and temp, Forward flow CO, CO_2 & H_2/H_2O number density.
10/6	169-228	100	1000	1.6	Forward flow N_2 number density and temp.
	229-266	100	1000	1.4	Forward flow N_2 number density and temp.
	267-311	100	1000	1.8	Forward flow N_2 number density and temp.
	312-371	100	1000	1.6	Forward flow N_2 number density and temp.
10/11	372-404	100	250	1.6	Backflow region N_2 number density and
10/12	405-437	100	250	1.6	temp. Pulse trains of 8 to 160 pulses
10/13	438-477	100	250	1.6	at 10 sec intervals.
10/18	478-520	varied	varied	varied	QCM mass flux measurements at 25°K.
10/19	521-547	100	100	1.6	Forward flow laser scattering - single pulse
	547-566	100	varied	1.6	Forward flow laser scattering - single pulse
	567-634	100	20	1.6	Forward flow laser scattering - single pulse
	635-659	100	100	1.6	Forward flow laser scattering - single pulse
	660-716	100	20	1.6	Forward flow laser scattering - double pulse
10/20	717-727	100	100	1.6	Forward flow laser scattering - single pulse
	728-748	100	20	1.8	Forward flow laser scattering - single pulse
	749-753	100	varied	varied	QCM mass flux measurements at 77°K.
	754-774	100	20	1.4	Forward flow laser scattering - single pulse
	775-787	100	20	1.6	Forward flow laser scattering - single pulse
	788-853	100	1111	1.6	Forward flow H_2 number density & temp. with modified optical system (Optical System II).

Table 2 Test Matrix for 9/22/78

Date/ Time	Firing No.	P_c (psia)	Pulse Width (ms)	Off Time (ms)	No. of Pulses	O/F Ratio	Remarks
9/22/78							
0950	55	100	1000	--	1	1.6	Performance
1030	56	100	1000	--	1	1.6	Performance
1125	57	100	1000	--	1	1.6	Performance
1220	58	100	250	--	1	1.6	Laser Scattering
1225	59	100	250	--	1	1.6	Laser Scattering
1235	60	100	250	--	1	1.6	Laser Scattering
1238	61	100	250	--	1	1.6	Laser Scattering
1340	62	100	250	--	1	1.6	Laser Scattering
1350	63	100	250	--	1	1.6	Laser Scattering
1353	64	100	250	--	1	1.6	Laser Scattering
1405	65	100	250	--	1	1.6	Laser Scattering
1409	66	100	250	--	1	1.6	Laser Scattering
1420	67	100	250	--	1	1.6	Laser Scattering
1423	68	100	250	--	1	1.6	Laser Scattering
1426	69	100	250	--	1	1.6	Laser Scattering
1429	70	100	250	--	1	1.6	Laser Scattering
1433	71	100	250	--	1	1.6	Laser Scattering
1436	72	100	250	--	1	1.6	Laser Scattering
1441	73	100	250	--	1	1.6	Laser Scattering
1444	74	100	250	--	1	1.6	Laser Scattering
1448	75	100	250	--	1	1.6	Laser Scattering
1458	76	100	250	--	1	1.6	Laser Scattering
1500	77	100	250	--	1	1.6	Laser Scattering
1503	78	100	250	--	1	1.6	Laser Scattering
1510	79	100	250	--	1	1.6	Laser Scattering
1515	80	100	250	--	1	1.6	Laser Scattering

Table 3 Mass Flux Data Record (typical)

DATE			10/18/78	10/18	10/18	10/18	10/18	10/18	10/18	10/18
Firing Number			481	483	484	485	486	487	488	489
T_x, ^oK			25.0	25.0	25.0	25.0	25.0	25.0	25.0	25.0
O/F			1.6	1.6	1.6	1.6	1.6	1.6	1.6	1.6
P_c, psi			100	100	100	100	100	100	100	100
δ, %			1.0	1.0	1.0	1.0	1.0	10.0	10.0	25.0
t_p, ms			100	100	50	20	10	20	20	20
N			100	50	100	250	250	200	100	100
QCM No.	ϕ,deg	r,cm	I,gm/sr-sec							
1	72.0	85.2	3.58 -2	3.11 -2	3.35 -2	4.50 -2	6.33 -2	4.19 -2	4.25 -2	3.01 -2
2	97.0	75.0	---	5.74 -3	5.68 -3	7.68 -3	---	---	---	---
3	83.0	77.5	2.18 -2	2.06 -2	2.20 -2	3.04 -2	4.28 -2	2.74 -2	3.06 -2	2.70 -2
4	107.	68.0	3.05 -3	3.01 -3	3.11 -3	3.99 -3	5.47 -3	3.56 -3	4.09 -3	3.43 -3
5	90.0	75.0	1.25 -2	1.15 -2	1.18 -2	1.60 -2	2.27 -2	---	1.63 -2	1.41 -2
6	121.	58.0	1.26 -3	1.46 -3	1.58 -3	2.10 -3	2.81 -3	1.83 -3	2.12 -3	1.76 -3
7	62.5	91.0	7.56 -2	7.71 -2	8.30 -2	1.13 -2	1.55 -1	1.06 -1	1.16 -1	1.02 -1
8	50.0	104.	1.52 -1	1.55 -1	1.63 -1	2.36 -1	3.43 -2	---	2.22 -1	2.17 -1
9	--	--	---	---	---	---	---	---	---	---
10	0.0	195.	1.08 -1	2.31 -1	2.90 -1	4.72 -1	6.14 -1	4.92 -1	2.04 -1	1.48 -2
11	135.	28.0	1.93 -4	1.86 -4	2.03 -4	3.08 -4	4.83 -4	2.88 -4	3.47 -4	2.85 -4